FAST FISSION RATIO CALCULATIONS

FAST FISSION RATIO CALCULATIONS

By:

Henri Paul Archer, B.Sc.

A Project Report
Submitted to the School of Graduate Studies
In Partial Fulfillment of the Requirements
For The Degree
Master of Engineering
McMaster University

1978 August

MASTER OF ENGINEERING (1978) McMASTER UNIVERSITY
Hamilton, Ontario

TITLE: Fast Fission Ratio Calculations

AUTHOR: Henri Paul Archer, B.Sc. (U.N.B.)

SUPERVISOR: Peter M. Garvey

NO. OF PAGES: X, 53

ABSTRACT

The precise knowledge of the Fast Fission Ratio is of considerable importance in Reactor Physics due to its effect on the overall reactivity of a nuclear reactor. Calculations obtained with the codes WIMS and LATREP disagreed by as much as 3% with experiments performed in the Zed-II critical facility of the Chalk River Nuclear Laboratories. It was felt that this variation might be due to the coarsity of the energy mesh since the energy range where Uranium (238) fission occurs (.8 to 10 MeV) was covered by only a few energy groups.

Two multigroup cross-section libraries having respectively 100 and 46 groups were therefore generated with SUPERTOG. Values for the Fast Fission Ratio were then calculated using first the one dimensional transport code ANISN and the Monte Carlo code MORSE. The 28 element fuel bundle geometry was used and the thermal fission was inputted to the codes as a fix source leaving to the codes the calculation of the activities in the upper groups of the multigroup structure (above 500 KeV). The cross-section data was obtained from the ENDF/B-IV library produced by the Brookhaven National Laboratory, U.S.A.

It was found that the WIMS energy structure with six groups above 500 KeV offered a sufficiently small energy mesh. In ANISN both the order of the angular quadrature (SN) and of the Legendre approximation to the scattering cross-sections (PN) were investigated. It was found that as SN increases the Fast Fission Ratio distribution across the fuel bundle flattens, approaching the distribution measured experimentally in Zed-II, while as PN increases the overall value of the Fast Fission Ratio increases leaving the distribution relatively unaffected.

Cases where the coolant has been received and replaced by air have also been investigated. This simulates what would be happening to the Fast Fission Ratio in the event of a total loss of coolant accident (LOCA). It was found that the Fast Fission Ratio would increase by about 15%. This represents a substantial positive contribution to the reactivity of the reactor.

Geometry effects were also investigated using the code MORSE. In this code the full two-dimensional pin distribution of the fuel bundle could be represented as opposed to the one dimensional smeared annuli model which had to be used in ANISN. However, it was found that this did not improve the results since a 3% decrease was observed in the absolute value of the Fast Fission Ratio while its distribution became slightly steeper than what was measured experimentally.

Two lattice pitches were also investigated, namely 24 and 28 cm. It was found that the tighter pitch led to an increase in the Fast Fission Ratio of the order of 5% without significant effect on the distribution.

The results obtained for the estimation of the Fast Fission Ratio with these Reactor Physics codes do not agree to better than 5% with the values determined experimentally. However, if one considers the experimental errors and the fact that the cross-sections are not known to better accuracies than a few percent, especially for Uranium (238) inelastic scattering, the results obtained are quite justifiable.

ACKNOWLEDGEMENT

I wish to express my gratitude to Mr. Peter M. Garvey from the Reactor Physics Branch of the Chalk River Nuclear Laboratories for both the design of this project and the supervision received. I am also grateful to both the Atomic Energy Commission of Canada and McMaster University for the arrangement allowing me to pursue this project as an industrial intern at the Chalk River Nuclear Laboratories.

I would also like to thank the personnel of the Chalk River Computing Center, particularly Mr. Peter Wong, for their assistance in some of the technical computting aspects of this project. Special mention should also be made to Professor A.A. Harms for coordinating my program of studies.

TABLE OF CONTENTS

ANALYSIS:

LIST OF FIGURES

LIST OF TABLES

NOMENCLATURE

Sn:	order of the angular quadrature used in discrete ordinate method
Pn:	order of Legendre approximation to the anisotropic scattering cross-section
γ:	fast yield ratio (FYR)
δ:	fast fission ratio (FFR)
ε:	fast fission factor (FFF)
θ:	(N,2N) reaction ratio (N2NR)
E:	energy
r:	radial dimension
ϕ:	neutron flux
N^{238}:	atomic density of uranium 238
σ_f:	microscopic fission cross-section
λ^{238}:	fission yield of uranium 238
W_g^R:	total yield in region (R) and energy group (G)
Q_R:	fix source input for fuel region (R)
χ:	fission neutrons energy spectrum (F.S.)

INTRODUCTION

The object of the present project is to determine value for the Fast Fission Ratio using Reactor Physics codes and to compare them with experimental values obtained in the CRNL Zed-II reactor.

The fast yield ratio (γ) is given by the following equation:

$$\gamma = \frac{\int_{fuel} dV \int_o^\infty dE\ n^{238}\nu^{238}(E)\sigma_f^{238}(E)\phi(r,E)}{\int_{fuel} dV \int_o^\infty dE\ n^{235}\nu^{235}(E)\sigma_f^{235}(E)\phi(r,E)}$$

while the Fast Fission Ratio (δ) is given by:

$$\delta = \frac{\int_{fuel} dV \int_o^\infty dE\ n^{238}\sigma_f^{238}(E)\phi(r,E)}{\int_{fuel} dV \int_o^\infty dE\ n^{235}\sigma_f^{235}(E)\phi(r,E)}$$

The Fast Fission Ratio can be related to the Fast Fission Factor (ε) which is given by:

$$\varepsilon = \frac{\int_{fuel} dV \int_o^\infty dE\ (n^{235}\nu^{235}(E) + n^{238}\nu^{238}(E)\sigma_f^{238})\ \phi(r,E)}{\int_{fuel} dV \int_o^{E_2} dE\ (n^{235}\nu^{235}(E)\sigma_f^{235}(E) + n^{238}\nu^{238}(E)\sigma_f^{238})\ \phi(r,E)}$$

$$\simeq 1+\gamma$$

where E_2 = 500 KeV is the fast reaction cut-off point.

The latter factor (ε) is one of the terms in the Four-Factor Formula for K_∞. Thus the knowledge of its exact value is of uppermost importance in reactivity calculations. Since it can be related to the Fast Fission Ratio (δ) according to the assumptions made in the theory used, it has become customary to publish values of (δ) since this is directly measurable.

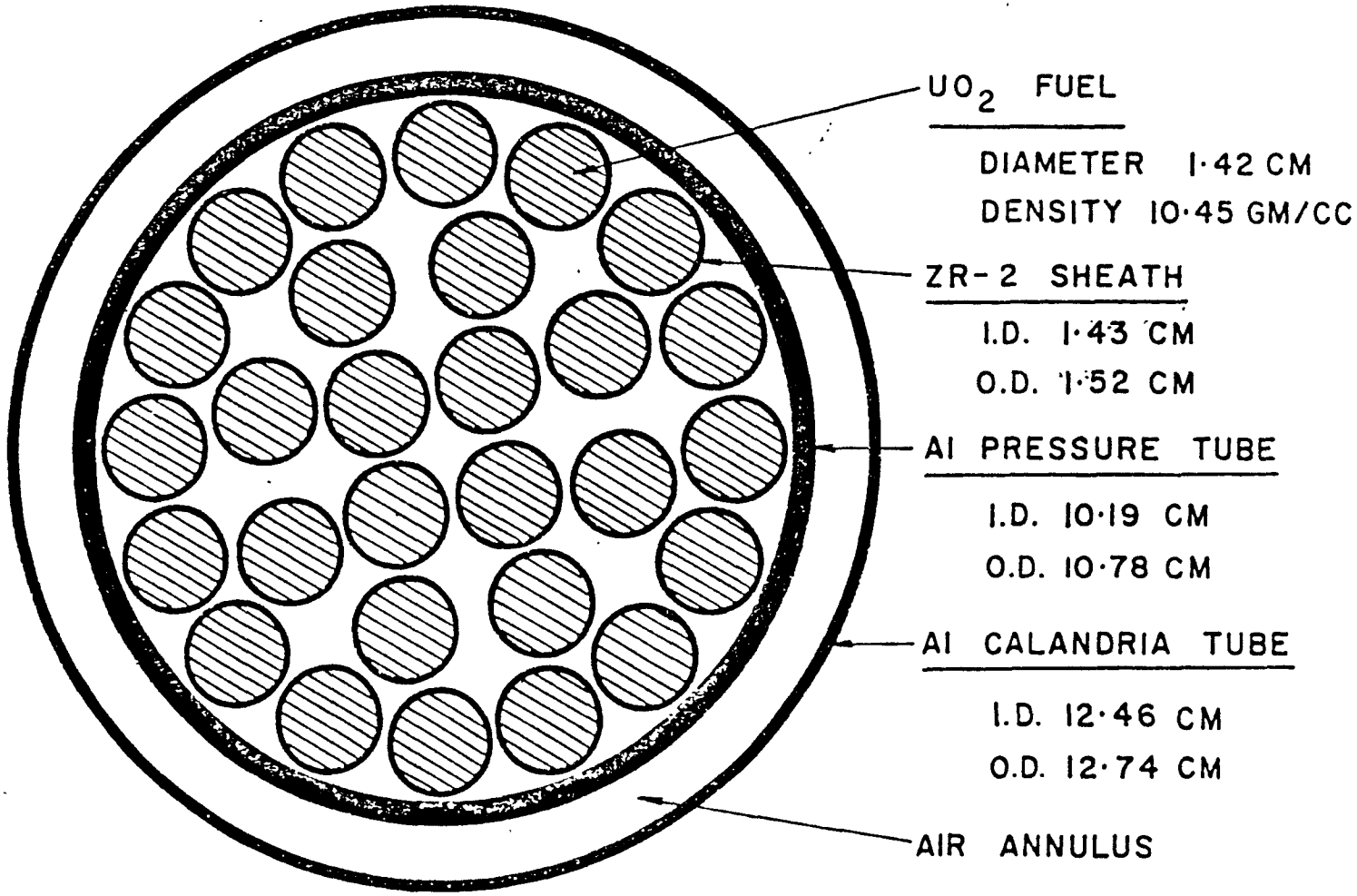

FIG. 1 28-ROD UO_2 FUEL ASSEMBLY

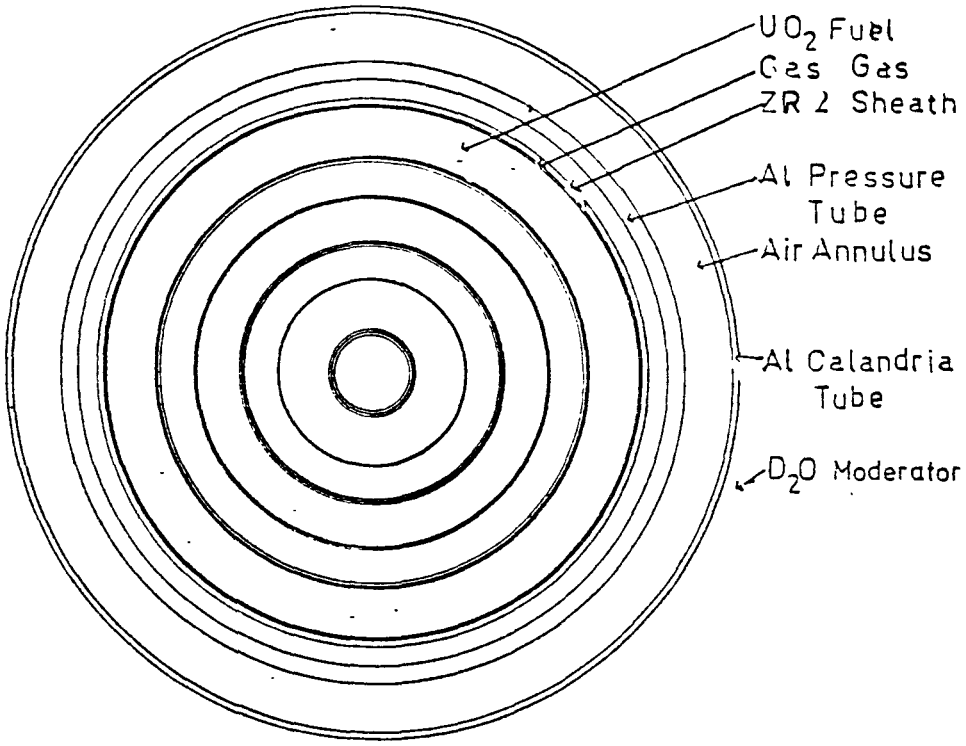

FIG. 2 :

Smeared Annuli Fuel Element Model

The way we will proceed in setting up our problem for both ANISN and MORSE will be to consider the thermal yield of U235 as a given parameter and input it as a fix source distributed in the fuel zones of our simulated 28 elements CANDU fuel bundle. These values are stated in AECL-2636 as determined experimentally in Zed-II.

We can then proceed to our energy structure and retain only the cross-sections above 500 KeV, considering the last energy group as a sink in which all the activities cross-sections including fission are set equal to zero. With this in mind we can then approximate the fast yield ratio (γ) and the Fast Fission Ratio (δ) in the following way:

$$\gamma = \frac{\Sigma_R \Sigma_g (n^{238} \nu^{238} \sigma_{fg}^{238} \phi_g^R)}{\Sigma_R \Sigma_g n^{235} \nu_g^{235} \sigma_{fg}^{235} \phi_g^R}$$

$$\delta = \frac{\Sigma_R \Sigma_g n^{238} \sigma_{fg}^{238} \phi_g^R}{\Sigma_R \Sigma_g n^{235} \sigma_{fg}^{235} \phi_g^R}$$

Where the integrations have been changed to summations over discrete energy and space mesh. Notice that the summation over the energy groups in the numerators only has to be done over the fast groups (above 500 KeV) since the U238 fission cross-section has a threshold above that energy. Also notice that the denominator is simply our input fix source, whose distribution among the different fuel regions we know. The numerator we can determine from the activities edit of the codes since they were operating precisely in those energy groups. For MORSE a little more work is involved to isolate the U235 yield and fission activities since only the total yield is given as output. However, with the knowledge of the fission and yield cross-sections for U235 and U238 and also their relative abundances it becomes possible to isolate the activities desired.

If we let (W_g^R) be the total yield in region (R) and energy group (G) we have:

$$W_g^R = (n^{235}\nu_g^{235}\sigma_{fg}^{235} + n^{238}\nu_g^{238}\sigma_g^{238})\ \phi_g^R$$

We can then express the Fast Fission Ratio (δ) and the fast yield ratio (γ) in the following way:

$$\gamma = (\Sigma_R\Sigma_g \frac{n^8\ \nu_g^8\ \sigma_{fg}^8 W_g^R}{n^5\ \nu_g^5\ \sigma_{fg}^5 + n^8\ \nu_g^8\ \sigma_{fg}^8}) \div (\Sigma_R Q_R)$$

$$\delta = (\Sigma_R\Sigma_g \frac{n^8\ \sigma_{fg}^8 W_g^8}{n^5\nu_g^5\sigma_g^5 + n^8\nu_g^8\sigma_g^8}) \div (\Sigma_R\ \frac{Q_R}{\nu^{235}})$$

$$Q_R = \Sigma_g n^{235}\nu_g^{235}\phi_g^R$$

where Q_R is our fix source by fuel regions.

ANISN is a discrete ordinate one dimensional code applicable to simple geometries like concentric circles in which you can define a radial axis. Since a CANDU fuel bundle consists of individual pins one has to establish a smeared annuli model to simulate it with ANISN. Due to the geometry of the 28 elements fuel bundle it is quite adequate to represent it as 3 concentric fuel annuli having the same center radius as the radius going through the center of the pin it represents. The 4 inner pins become the first inner annuli, the 16 outer pins become the outer annuli and the 8 remaining pins the center annuli. The volume of UO_2 fuel, air gap and zirconium cladding has to be conserved. The further assumption that there are equal thicknesses of materials on each side of those three radii going through the center of the pins was made for most cases.

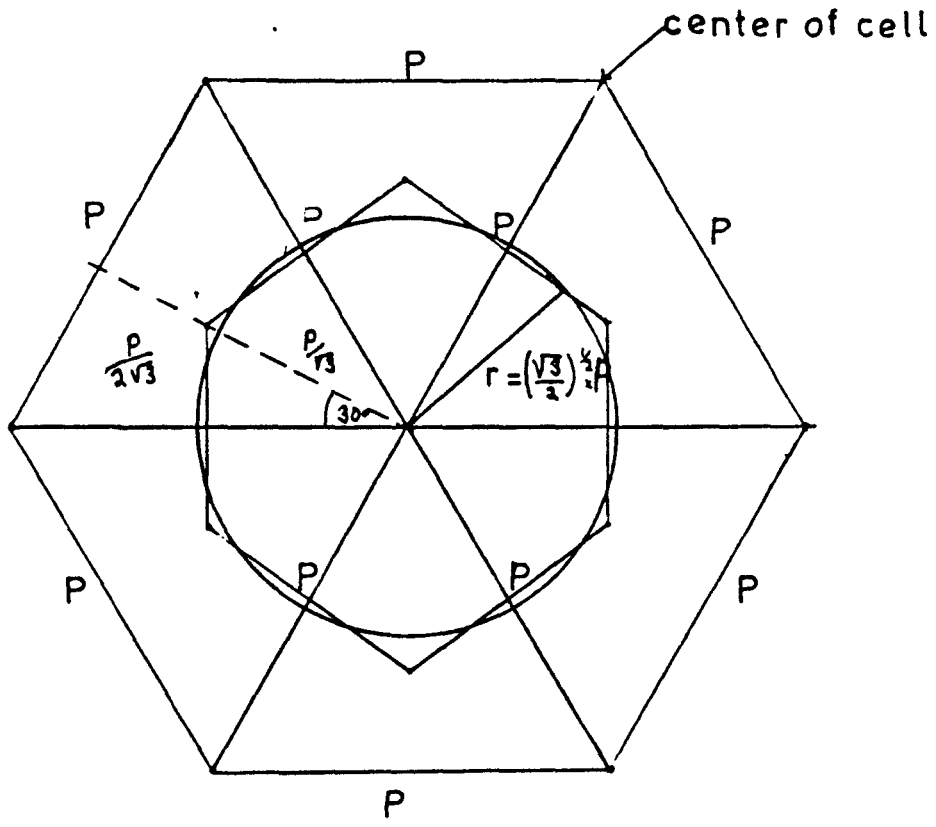

Triangular Lattice Arrangement

FIG.3: Diagram showing how the moderator radius is assigned to the fuel cell as a function of the lattice pitch.

However a more exact case where the area below that centers circle in the pin was conserved in the annular model was investigated.

The Reactor Physics code MORSE which is a Monte Carlo code was also used. More complex geometries can be used here since it is a full three dimensional code. The exact pin distribution was therefore investigated. The smeared annuli model was also simulated with ANISN results. Fix sources for MORSE are inputted in the form of one particle at a time which has been randomly generated according to the distribution in which they were experimentally found to occur. Tapes containing data for 100,000 such particles have been generated.

The previously mentioned codes also need multi-group cross-section libraries. The CANDU bundles can be represented using seven elements. Cross-section data for these materials is available from the ENDF/B-IV tapes. They were weighed in to a set of group cross-sections according to the particular energy structure and a fission spectrum joined to an epithermal flux. This does represent quite closely the flux versus energy spectrum in a fuel bundle.

PROCEDURE

The CANDU fuel bundle can be adequately represented from the material point of view with the seven following elements:

1. Aluminum (^{27}Al)
2. Zircaloy-II (Zr-2)
3. Oxygen (^{16}O)
4. Uranium isotope (^{235}U)
5. Uranium (^{238}U)
6. Hydrogen (^{1}H)
7. Deuterium (^{2}D)

Cross-sections data for these elements are available from the ENDF-B tapes. These cross-section libraries are produced by Brookhaven National Laboratory, USA. They are periodically updated as new experimental data becomes available. The version used was updated as of 1974 June.

The program SUPERTOG was used to read the data from these tapes and produce cross-sections libraries for both the GAM-II (100 groups) energy mesh and the WIMS (46 groups) energy mesh. A weighting function of 1/E joined to a fission spectrum was used. Modifications had to be made to SUPERTOG so that it could generate scattering matrices for materials like (^{1}H) for which the Legendre expansion coefficients (Pℓ) for the scattering matrices are not available on the ENDF-B tape.

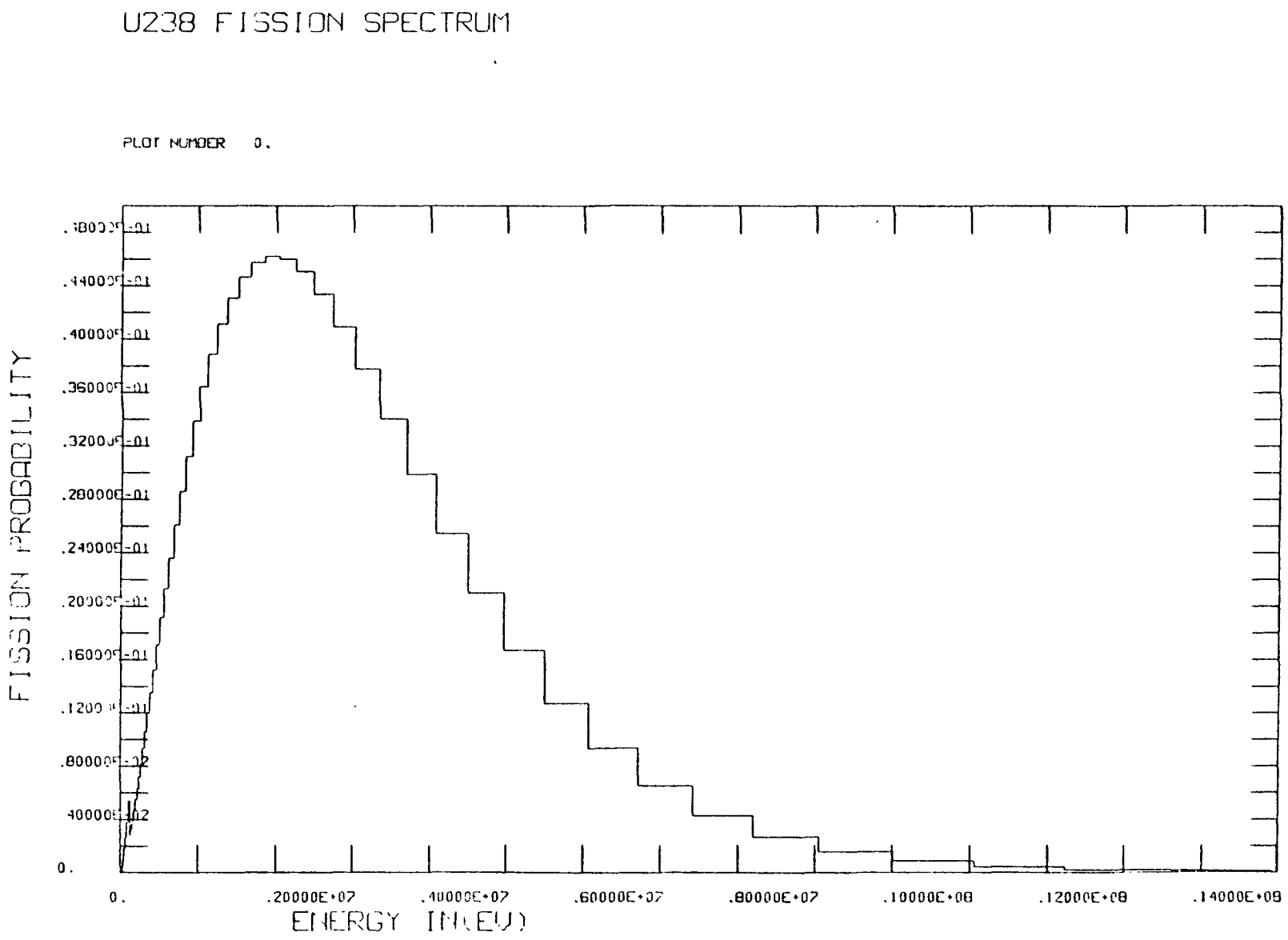

FIGURE 4: U238 Fission Spectrum

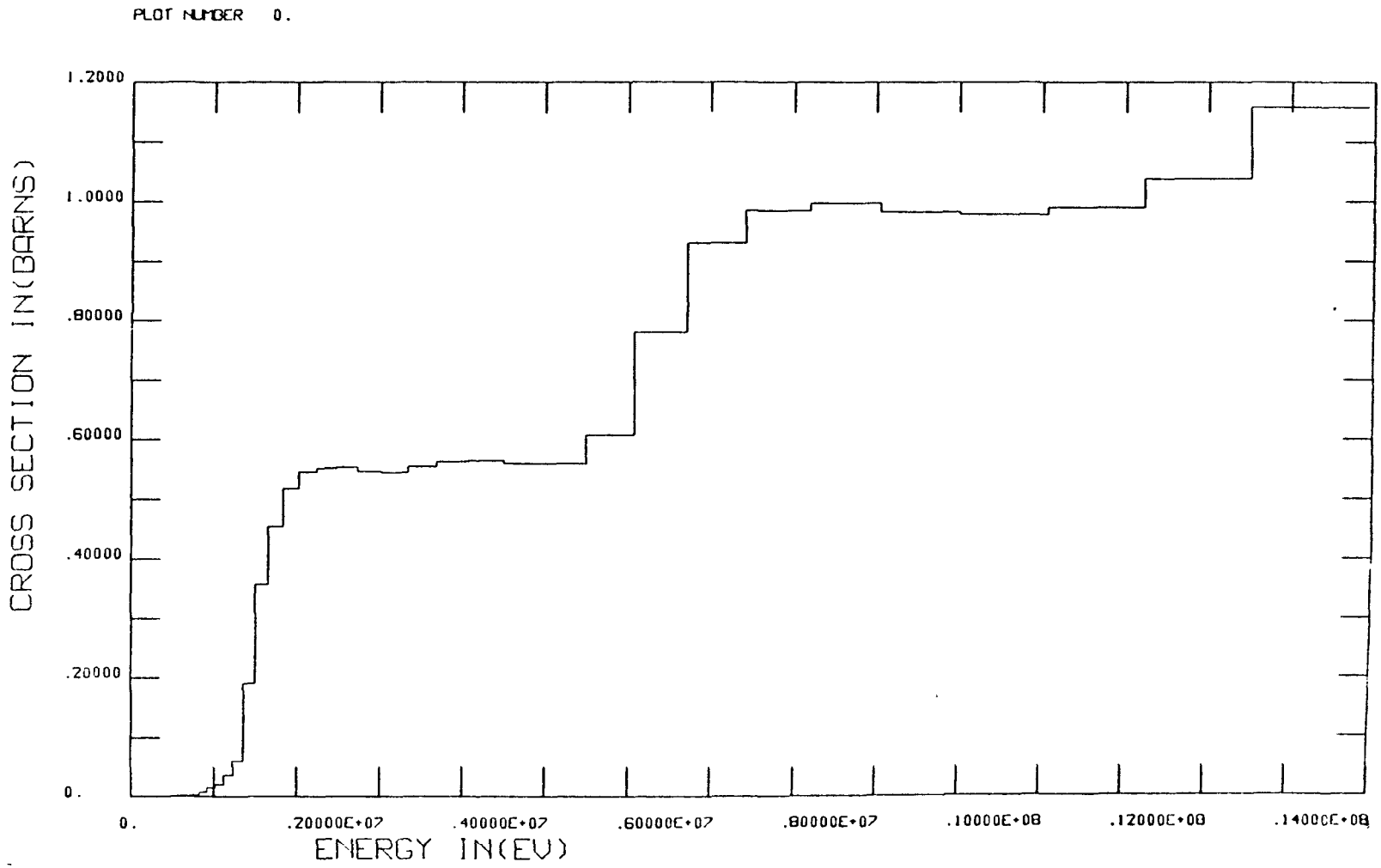

FIGURE 5: U238 Fission Cross-section Spectrum

This was achieved by adding the subroutines LEGEND and LECOM and modifying GADD, all of which were obtained from a previous version of SUPERTOG called ETOG. It involved a few dimension and logic flow changes in the main program. Problems were also encountered while processing data for ^{16}O under the WIMS energy group structure. There were too many data points in group #5 having an energy range from 4.85 MeV to 6.23 MeV. The dimensions in SUPERTOG could not accommodate more than 100 points while there were 150 on the tape. The solution used was to remove every third point in the data set using the fortran routine REDUCER.

The cross-sections of the seven elements (SUPERTOG output) were then assembled into one cross-section library using the program FORMATER. Two cross-section libraries, GAM-II and WIMS were thus created. They were written in the ANISN card image format including six activity cross-sections at the beginning of the data for every material. These libraries have Legendre coefficients up to the order of P8. The program DLC-2 was then used to reduce these cross-section libraries from 100 groups to 34 groups and from 46 groups to 6 groups. Thus the libraries contain only data upwards from 500 KeV. The last group of these libraries was modified so that it would constitute a sink group with zero activity, no down scattering and a self-scattering cross-section equal to the total cross-section minus the absorption cross-section.

DLC-2 wrote its results on an unformatted (binary) tape, catalogued as DATAW for the 6 group library and as DATAF1 for the 34 group library. These two permanent files are group dependent cross-section libraries containing 9 materials for every element (i.e. one for every Legendre order (P_0 to P_8). For each material the data is ordered as follows:

Position	Activity
1	(n,n) elastic scattering
2	(n,n^1) inelastic scattering
3	(n,2n)
4	(n,f) fission cross-section
5	$(n,n^1)\alpha$
6	(n,α)
7	σa absorption cross-section
8	$\nu\sigma_f$ yield cross-section
9	σ_T total cross-section
10	σ_{gg} self-scattering

The file DATAF1 (34 groups) was then processed through TAPEMAKER which outputs a group independent cross-section library. This final library was catalogued in its binary form under the name DATAFILE. This constitutes the input cross-section library for ANISN.

ANISN was run under the fixed source option. Fixed source tapes thus had to be prepared as input to ANISN. The source tape contains a number for every energy group and every space interval representing the probability of a 235 fission neutron emerging at that point in space and of that energy. The distribution of source neutrons with respect to space was obtained in the report AECL-2636 where it was stated for the three fuel annuli of the 28 element fuel bundles. It was set equal to zero outside those smeared fuel annuli. The distribution by energy groups was obtained from the U235 fission spectrum calculated from the ENDF-B data tapes with the program ETOG for an input neutron energy of .025 eV. A fission spectrum for U238 with an input neutron of 1 MeV was also obtained with ETOG. Note that ETOG, which is the earlier version of SUPERTOG, was used to generate the fission spectrums. This is because ETOG had an input variable to specify the input neutron energy.

The fission probability in the last group of the truncated energy structures (34 and 6 groups) had to be modified so that the fission probabilities by group for these truncated energy structures would add up to one. This was achieved using the program FSPEC. A smeared annuli model of the 28 element fuel bundles has to be calculated for input to ANISN. Since ANISN is a one dimensional code it cannot accept the exact pin distribution of the fuel bundle, as multi-dimensional codes like WIMS and MORSE can.

This smearing is done assuming that the four center fuel pins are one annulus of fuel, the eight next pins are a second fuel annulus and the sixteen outer pins are a third annulus. The annuli of fuel were assumed to be of equal thickness on each side of the radius that goes through the center of the pins involved. The area of fuel air gap and cladding must also be conserved. Other more involved smearing than equal thickness can also be used, like conserving the same area of fuel inside and outside the radius going through the center of the pins.

ANISN was run for different values of Legendre order of scattering (Pn) and different order of angular quadrature. Cases for both the 34 groups and 6 groups energy structure were run with both heavy water and air coolant. The same mesh spacing as the program LATREP was also used instead of the regular 56 interval mesh. For most of the runs normal reflection was used for both the left and the right boundary condition. Some cases were run with white reflection and albedos of 0.0, 15 and 1.0 for the right boundary condition.

The three dimensional Monte Carlo code MORSE was also used to study the geometry effects of the smearing of the bundle. For this code special fix sources tapes had to be prepared. They consisted of sequential data for specific input neutrons specifying their spacial position and their energy interval. The source tapes contain data for 100,000 particles. The pin distribution can also be simulated in exactly the same spacial distribution as they occur in the 28 element fuel bundle.

A fortran program called CALC was written to calculate fast fission ratios and (N,2N) reaction ratios from the "fission products counters" output of MORSE. (It uses as input the number of fixed source particles being inputted in each fuel ring). These values are corrected for the fact that source particles are only produced in the 5 upper energy groups. The U235 yield cross-section and the U238 yield and (N,2N) cross-sections for the first 5 groups are also provided as input to CALC.

These cross-sections were set to zero for group #6 which was the sink group.

ANALYSIS

(1) Values of the fast fission ratio (δ) were obtained with ANISN using both an energy mesh of 6 groups (WIMS structure) and of 34 groups (GAM-II structure). The fast fission ratio (δ) was found to vary by less than 1.0% for the two energy structures. The 6 group structure is therefore quite sufficient and was retained for the remaining calculations since it is much less cumbersome. The distribution of (δ) with respect to the 3 fuel rings also changed insignificantly between the two energy structures. We would also expect the values of (δ) to be slightly different between the two energy structures since the 34 groups structure had a top energy cut-off of 14.918 MeV.

(2) The effect of the Legendre order approximation (P_n) to the scattering cross-section was also investigated. Going from a P_3 approximation which is commonly used in Reactor Physics codes, to a higher order of P_8 had an effect on the fast fission ratio of between 3% and 4%, bringing its average value closer to the experimental value obtained in ZED-II. Approximations of P_8, P_1 and P_2 were also used. Table (I) containing cases #1,2,12,13,16 resumes the Legendre order approximation (P_n) investigation. All these ANISN cases used reflection for both the right and the left boundary conditions. An angular quadrature of the order S_4 was used in the 4 cases, the coolant was 99.78% heavy water and the 56 interval fix source was distributed among the 3 fuel rings as stated in the AECL-2636 report.

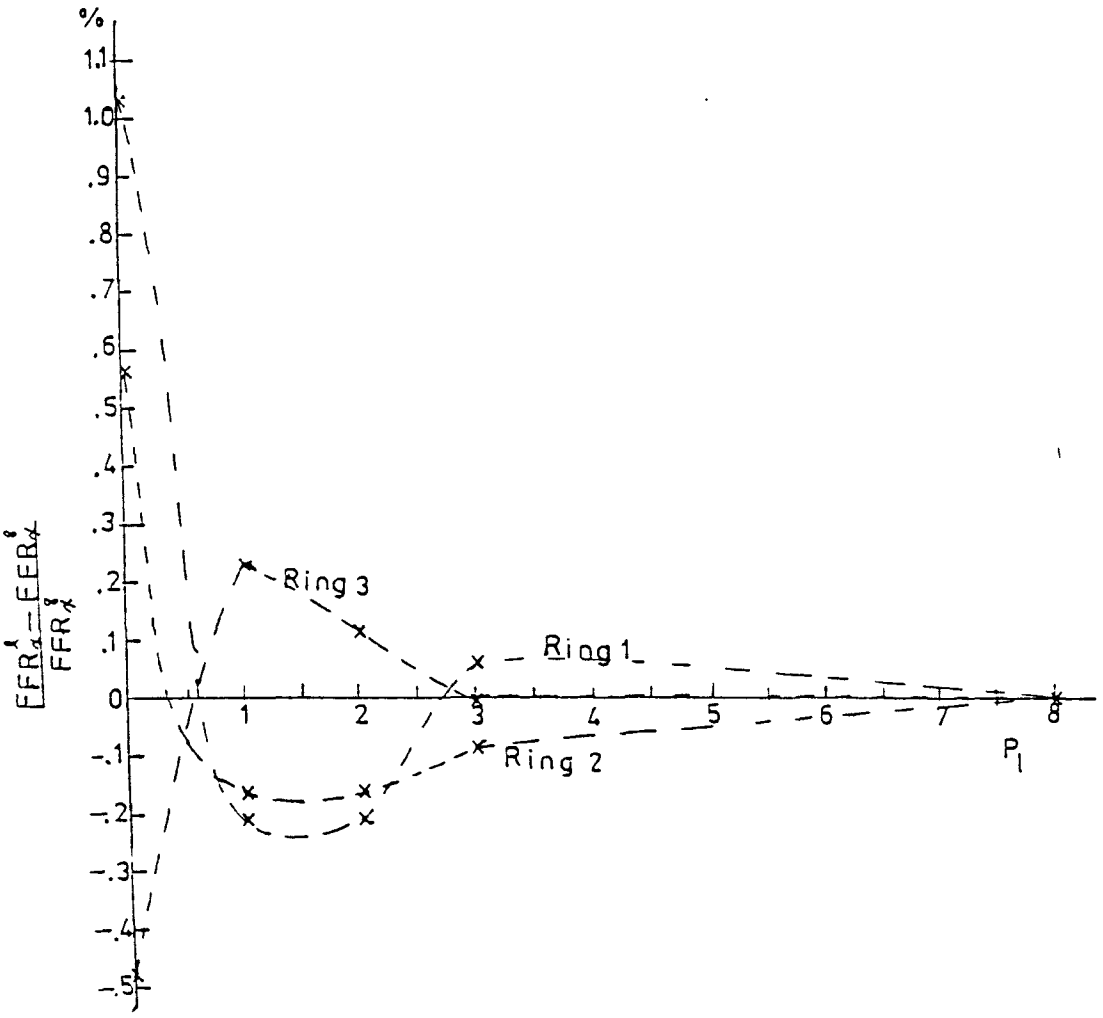

FIGURE 6: % Fast Fission Ratio versus P_l

Even though the P_0 case agrees best with the report value this is just a hazard since the value of (δ) seems to be oscillating about a converging value as the order increases. We can see that the difference between P_0 and P_1 is of the order of 10% while the difference between P_1 and P_2, and P_2 and P_3 is of the order of 2% and 1%. However, the difference in the distribution between the 3 fuel rings does not change very much except for the P_0 case. A straight diffusion case was also run, however the results obtained differ considerably from the report value or from the other cases.

(3) A typical feature of discrete ordinate theory is the use of an angular quadrature (Sn). Quadrature orders of 2,4,8,12 and 16 as published in a Westinghouse report were investigated. Table (II) shows the results of the relevant cases.

It can immediately be noticed that the effect of increasing the Sn order is to flatten the distribution across the 3 fuel rings without affecting much the absolute value of the average fast fission ratio as opposed to the Pn order which affects the absolute value without changing the distribution significantly. We can also see that the distribution seems to be converging slowly towards the experimental distribution as the order of the angular quadrature increases.

Case #3 was run with a 4th order angular quadrature obtained from Ref. (9), but varying slightly from the Westinghouse 4th order quadrature. It can be seen that a slight effect on the fast fission ratio distribution is obtained. Therefore confirming that some biased quadrature can be better for a particular problem.

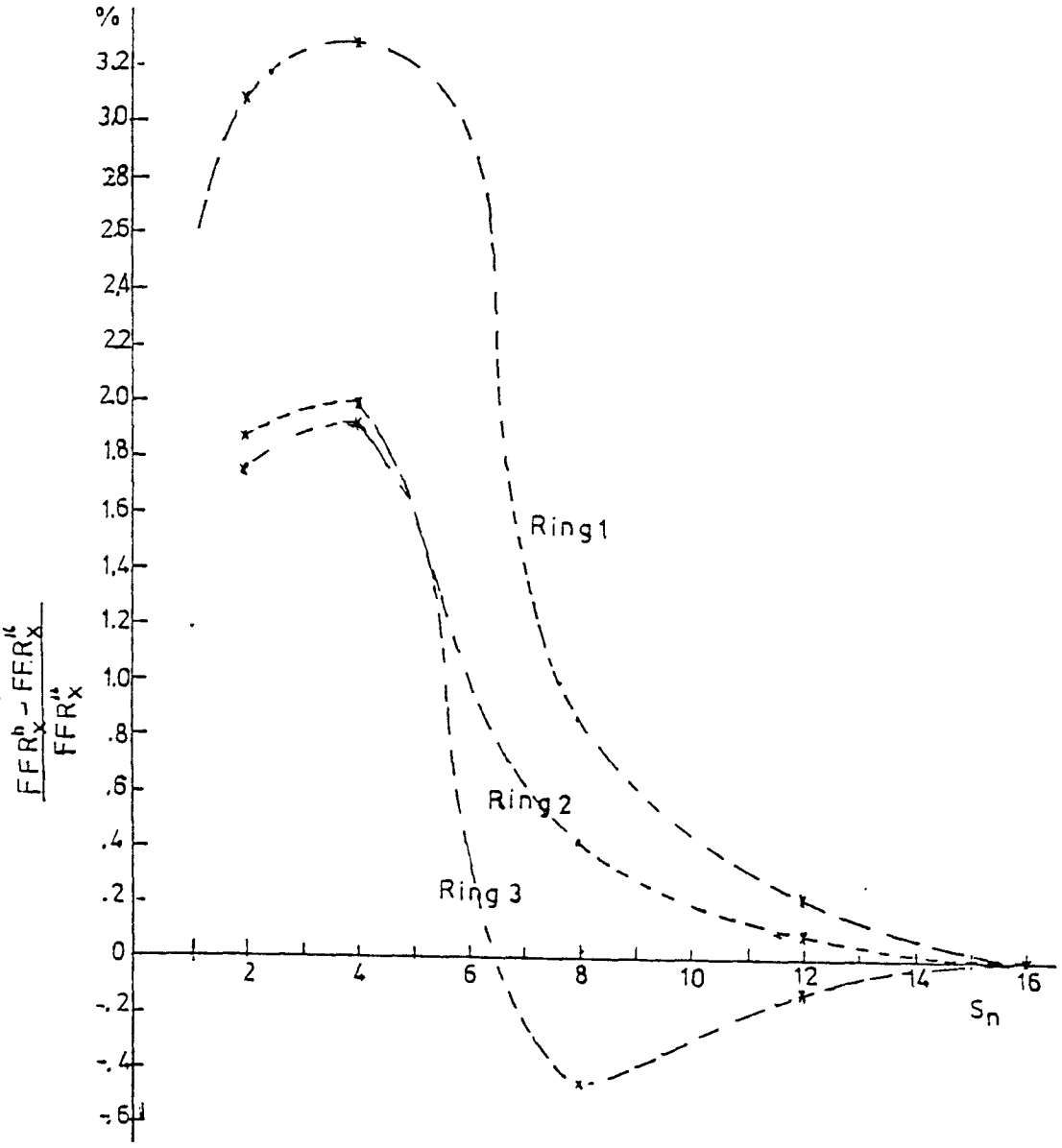

FIGURE 7: % Fast Fission Ratio versus S_n

TABLE I: Legendre Approximation Order

Case #	PN	FFR	FFR1/FFR	FFR2/FFR	FFR3/FFR	%DIFF.
12	0	.054	1.459	1.228	.833	6.75
13	1	.049	1.441	1.219	.839	15.8
16	2	.050	1.441	1.219	.839	13.7
1	3	.050	1.445	1.229	.837	14.2
2	8	.052	1.444	1.221	.837	11.2
18 DIFF		.035	1.518	1.253	.812	39.7
AECL-2636		.0582	1.368	1.180	.866	0.0

TABLE II: Angular Quadrature Order

Case #	SN	PN	FFR	FFR1/FFR	FFR2/FFR	FFR3/FFR	%DIFF.
16	2	3	.050	1.441	1.219	.838	13.7
2	4	8	.052	1.444	1.221	.837	11.2
10	8	8	.051	1.410	1.203	.850	11.7
9	12	8	.052	1.401	1.199	.853	10.8
30	16	8	.052	1.398	1.198	.854	10.4
3	4*	3	.051	1.436	1.216	.840	12.8
AECL-2636			.0582	1.368	1.180	.866	0.0

TABLE III: Right Boundary Condition

Case #	F.B.C.	FFR	FFR1	FFR2	FFR3	%DIFF.
1	Reflection	.050	1.445	1.220	.837	0.0
14	White/Alb=1.0	.050	1.447	1.221	.837	.7
17	White/Alb=0.0	.048	1.454	1.224	.834	3.5

TABLE IV: Hardened Fission Spectrum

Case #	COOL.	F.S.	FFR	FFR1/FFR	FFR2/FFR	FFR3/FFR
1	D_2O	238 (1MeV)	.050	1.445	1.220	.837
3	Air	238 (1MeV)	.058	1.382	1.282	.844
24	D_2O	235(.025eV)	.050	1.445	1.220	.837
25	Air	235(.025eV)	.058	1.381	1.282	.844

TABLE V: Transport Corrected Cross-sections

Case #	FISSION-SPEC.	SOURCE F.S.	COOL	FFR	FFR1	FFR2	FFR3
22	238 (1MeV)	.025eV	D_2O	.051	1.444	1.221	.837
28	238 (1MeV)	1.43MeV	D_2O	.056	1.444	1.221	.837
26	235(1.43MeV)	1.43MeV	D_2O	.056	1.445	1.221	.837
29	238 (1MeV)	1.43MeV	Air	.065	1.375	1.200	.846
27	235(1.43MeV)	1.43MeV	Air	.065	1.376	1.200	.846
30	238 (1MeV)	.025eV	D_2O	.052	1.398	1.198	.854

TABLE VI: Geometry Effects

Case #	GEOM.	COOL.	FFR	FFR1/FFR	FFR2/FFR	FFR3/FFR
17	ANN(ET)	D_2O	.055	1.334	1.166	.878
18	PIN	D_2O	.053	1.393	1.212	.850
AECL-2636		D_2O	.0582	1.368	1.180	.866

(4) A spacial mesh of 56 intervals was arbitrarily used for the ANISN cases. One case was also run with the 26 intervals LATREP mesh (Case 19). A lower value of the fast fission ratio (2.7% difference) and a steeper distribution was observed in Case #19. However, since the extra intervals for the 56 intervals mesh were added in the most significant zones like the fuel rings and the coolant and since the flux did not vary by more than 10% from interval to interval, it was felt that the 56 intervals mesh was quite adequate. This mesh was therefore used in all other ANISN cases.

(5) The effect of the right boundary condition was also considered. The relevant cases here are #1, 14 and 17.

For the left hand boundary condition reflection was used throughout all cases since it was dictated by the symmetry of the center of the fuel bundle. It can be seen from the above table that the difference between a reflective and a white with Albedo equal to 1.0 right hand boundary condition is not very significant. This is to be expected since the White/Albedo=1.0 condition is simply an isotropic reflection and due to the cylindrical shape of the fuel bundle there should be a slight bias of the reflection therefore varying from isotopic reflection. However, with an Albedo of zero, meaning that all particles reaching the boundary leak out of the system as would be the case for a single cell reactor as opposed to an Albedo of one which would be the case for an infinite array of cells, the results vary significantly both in absolute value and distribution. The distribution of the fast fission ratio becomes steeper, that is there is relatively more fast fission in the center of the bundle than in the outer fuel ring while the absolute value of (δ) goes down by about 3.5%. This result is obvious since more fast neutrons will be lost by the system for an Albedo of zero and the region which will suffer the most from neutrons not being reflected as far as fast fission is concerned is the outer ring of fuel.

(6) Hardened Fission Spectrum:

Many programs generate all new generation neutrons according to the U235 fission spectrum, neglecting that some of those neutrons were produced by U238 fission. However, as it can be seen in data table (IV), there is a slight difference in the fast fission ratio if the U238 fission spectrum is used.

(7) Transport Corrected Cross-sections Cases:

If we first compare case #22 with #30 we see that the absolute difference in the fast fission ratio when going to a transport corrected cross-section library is only of 1.4%, however, the distribution is considerably steeper. By looking at case #28 we can see that if we hardened the U235 fission spectrum in the fix source we can increase the fast fission ratio by as much as 8.5% without affecting its distribution. If we further hardened the fission spectrum for the fast groups convergence we can bring the fast fission ratio up by 10% which agrees very well with experiments, however the distribution remains unchanged. This artifice has been used in WIMS to yield the proper absolute value of the fast fission ratio. Note that we saw in part (6) the difference from a U238 fission spectrum to a U235 fission spectrum was quite small.

(8) The program MORSE was used to investigate the geometry effects. Table (VI) shows the most relevant cases. We immediately observe that going from an equal thickness approximation to a more accurate part of circles approximation does not have very much effect on the absolute value of the fast fission ratio but it has a large influence on its distribution. As for the exact pin distribution it shows an approximately 3% decrease in the absolute value of the fast fission ratio and the distribution has a slightly steeper gradient as you go from the center of the fuel bundle to the outside. Attempts were also made to study a square moderator, but due to bugs in the code MORSE it was unsuccessful.

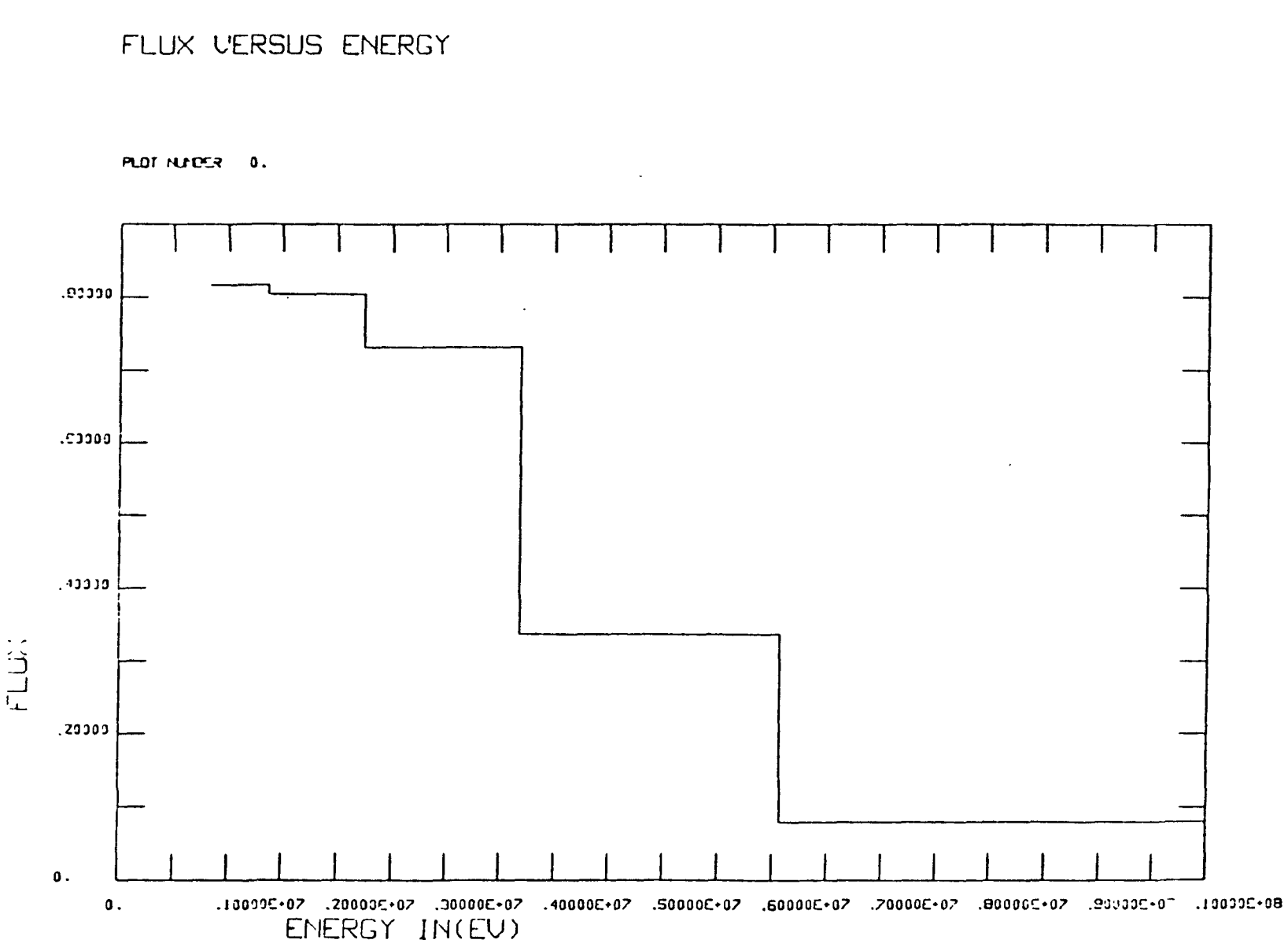

FIG.8: Normalized neutron flux for the 5 upper energy groups in a CANDU bundle.

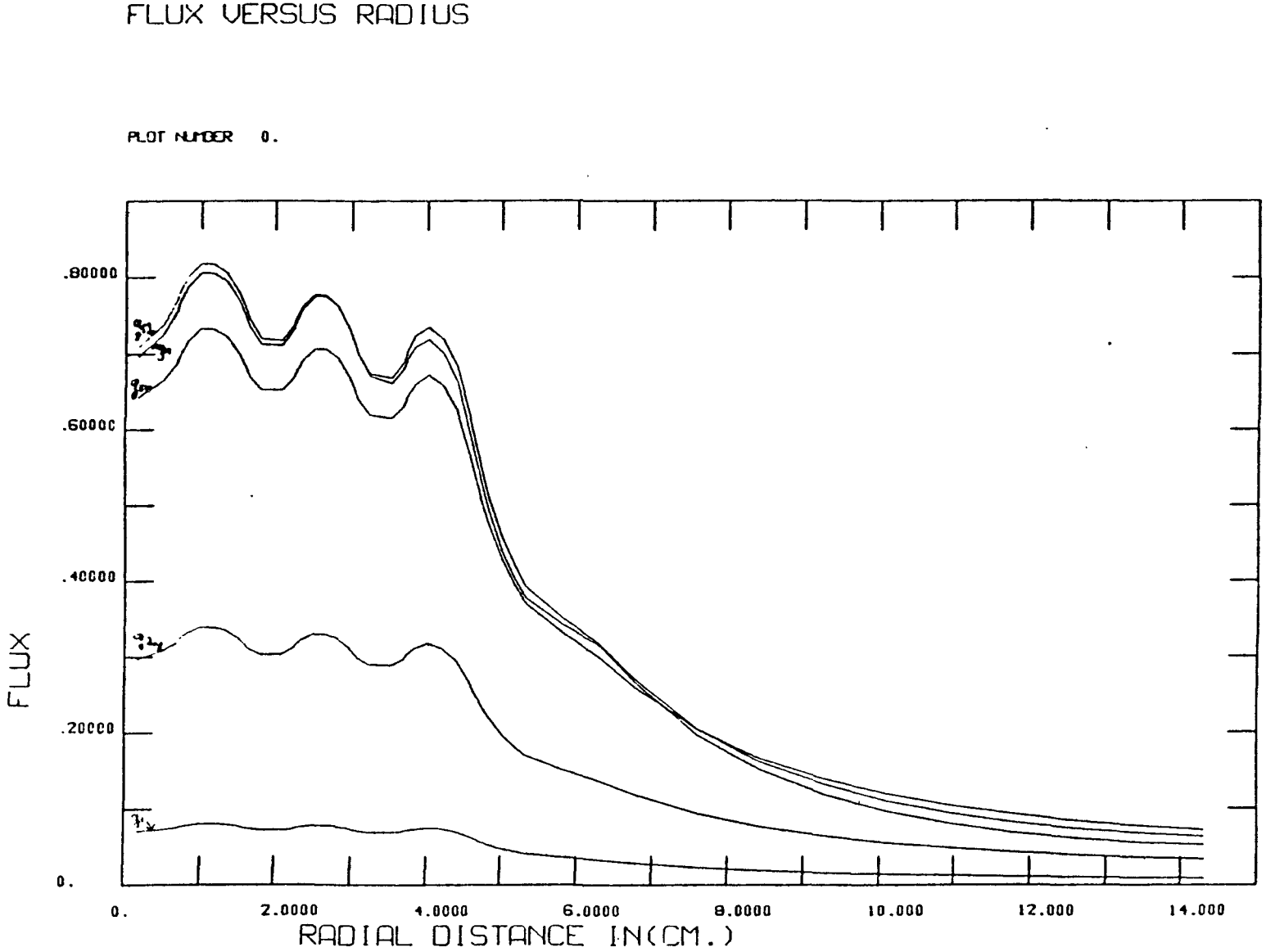

FIG.9 : Flux for the 5 upper energy groups across a 28 element fuel bundle.

(9) Cases with the heavy water coolant removed were also simulated. These so called air coolant runs allow us to look at what would happen to the fast fission ratio in a loss of coolant accident (LOCA). The fast fission ratio is then of the order of 20% higher, thus contributing as a substantial positive reactivity. The air coolant cases gave results much closer to the experimental values obtained in ZED-II. The fast fission ratio distribution for air coolant is also flatter as was found experimentally.

A different lattice pitch has also been investigated. All the cases referred to above had a pitch of 28 cm. Thus a moderator thickness of 8.351 cm associated with the cell. The other pitch considered was of 24 cm for a moderator thickness of 6.251 cm. This lattice tightening leads to an increase in the fast fission ratio of the order of 5% without much effect on the distribution.

In general, the values for the fast fission ratio obtained with MORSE are a little over 5% higher than the value obtained with ANISN for the highest values of the angular quadrature and of the Legendre approximation.

(10) WIMS Calculations

#	GEOM.	COOL.	TYPE	TIME	FFR	FFR_1	FFR_2	FFR_3
1	DSN	D_2O	INF	13.062	.04941	1.478	1.205	.838
			EFF		.05480	1.476	1.205	.839
2	DSN	AIR	INF	12.089	.05580	1.414	1.197	.845
			EFF		.06220	1.412	1.196	.845
3	PIJ	D_2O	INF	73.538	.04899	1.426	1.190	.850
			EFF		.05401	1.405	1.193	.853
4	PIJ	AIR	INF	14.248	.05483	1.343	1.188	.858
			EFF		.06091	1.342	1.187	.858

TABLE VII: WIMS Calculations

The results in Table 7 were obtained using the transport code WIMS. It uses transport corrected cross-sections of Legendre order Po. As Table 7 shows the code gives a k_∞ and a $k_{effective}$ reaction edit. The $k_{effective}$ is the one that is close to experiments and also compares best with the results from MORSE and ANISN. WIMS works under two different options, the DSN (discrete Sn method), one dimensional, and the PIJ multidimensional method. Both air and D_2O coolant cases have been run using both methods. The difference in the fast fission ratio given by the k_∞ and the $k_{effective}$ edit is of the order of 10%, $k_{effective}$ giving the most realistic value. The difference in the overall fast fission ratio between the D_2O and the AIR coolant is of the order of 13% higher for the loss of coolant case. The differences between the annular and the pin geometries are rather small, 1.5% for the D_2O coolant and 2.1% only for the AIR coolant. The distributions across the different fuel regions are however, very much affected. It is steeper in the annular geometry than in the pin geometry, unlike what was found in MORSE. The distributions for the k_∞ and $k_{effective}$ edits are essentially the same. Again the distributions of the AIR coolant cases are flatter than those of the D_2O coolant.

(11) Two different energy structures were used with the code ANISN. One contained 6 energy groups above 500 KeV (WIMS structure) and the other contained 34 groups above 500 KeV (GAM-II structure). The (N,2N) ratio found with the GAM-II structure is about 13% higher than what was calculated with the WIMS structure. This can be explained by the fact that the tighter structure had an upper bound of 14.918 MeV as opposed to 10 MeV for the WIMS structure. (N,2N) reactions have an upper bound of about 18 MeV, but the flux above 10 MeV in a CANDU reactor is very small.

(12) The effect of the order of the Legendre expansion (Pn) to the anisotropic scattering matrices was also investigated. Table VIII shows the relevant ANISN cases which used reflection for both the right and the left boundary conditions. An angular quadrature of order S_4 was used in the 4 cases, the coolant was 98.70 p.c. heavy water and the 56 intervals fixed source was distributed among the 3 fuel rings as stated in the AECL-2636 report.

Case #	Pn	N2NR(%)	$N2NR_1/N2NR$	$N2NR_2/N2NR$	$N2NR_3/N2NR$
12	0	.10201	1.448	1.226	.834
13	1	.09470	1.426	1.215	.843
16	2	.09694	1.428	1.216	.842
1	3	.09608	1.433	1.217	.841
2	8	.10857	1.426	1.221	.841

TABLE VIII: Legendre Approximation Order

As for the fast fission ratio, the absolute value of the ratio increases slightly for high order of Pn and the distribution flattens as you travel from the center of the fuel bundle to its outer pins. Note that there are more (N,2N) reactions in the center of the bundle since the flux is harder there.

(13) Since ANISN is a discrete ordinate code the effect of the order (Sn) of the angular quadrature on the (N,2N) reaction ratio was also considered. TABLE VIII shows us results for the relevant cases.

Case #	Sn	N2NR(%)	$N2NR_1/N2NR$	$N2NR_2/N2NR$	$N2NR_3/N2NR$
15	2	.13110	1.419	1.195	.851
2	4	.10857	1.426	1.221	.841
10	8	.10039	1.394	1.199	.854
9	12	.10200	1.385	1.195	.857
30	16	.10302	1.383	1.194	.858
3	4*	.09771	1.424	1.213	.844

TABLE IX: Angular Quadrature Order

The N2N ratio varies only slightly in average value over the whole fuel bundle for different Sn order. However, its distribution across the fuel bundle seems to flatten with higher Sn orders. Case #3 is using a different 4th order quadrature obtained from the Savannah River Laboratory Report #DPST-70-233 and varying slightly from the other angular quadratures obtained from a Westinghouse report. It can be seen that it leads to a slight effect on the (N,2N) ratio which confirms that some biased quadrature can be better for a particular problem.

(14) Due to the symmetry of the CANDU fuel bundle, cylindrical geometry was used in all the ANISN cases. Only the radial dimension was considered using a reflective left hand boundary condition at the center of the bundle. However, different right hand boundary conditions were used. Table (X) shows the effect of these different boundary conditions on the N,2N ratio:

Case #	R.B.C.	N2NR(%)	$N2NR_1/N2NR$	$N2NR_2/N2NR$	$N2NR_3/N2NR$
1	Reflection	.09608	1.433	1.217	.841
14	W/Alb=1.0	.09492	1.435	1.218	.840
17	W/Alb=0.0	.09119	1.445	1.223	.836

TABLE X: Right Boundary Condition

The white boundary condition simply means isotropic reflection which can vary slightly from pure reflection since the latter can have some bias according to geometry. A difference is observed in the magnitude of the N,2N ratio, the reflection and the W/Alb=1.0 boundary condition, but no difference is seen in its distribution in the three fuel rings. A further decrease in the N,2N ratio is seen when going from an albedo of 1.0 (every incident neutron reflected) to an albedo of 0.0 when no reflection occurs and all neutrons reaching the outer boundary leak out of the system. However, the difference is not as significant as one might first think since there is a portion of heavy water moderator between the fuel rings and the right hand boundary so that most neutrons will not have enough energy after going through it to cause (N,2N) reactions. The distribution of (N,2N) reactions is also steeper for an albedo of zero since there are no neutrons from reflection being added to the outer fuel pins.

(15) Hardening of the fission spectrum is a technique that has been used in some Reactor Physics code to obtain higher reaction rates. Table (XI) shows its effect on (N,2N) reactions.

Case #	Cool	F.S.	N2NR(%)	$N2NR_1/N2NR$	$N2NR_2/N2NR$	$N2NR_3/N2NR$
1	D_2O	238 (1 MeV)	.09608	1.433	1.217	.841
4	Air	238 (1 MeV)	.10919	1.469	1.232	.828
24	D_2O	235 (.025 eV)	.09630	1.433	1.217	.840
25	Air	235 (.025 eV)	.10947	1.369	1.197	.849

TABLE XI: Hardened Fission Spectrum

The effect on the overall reaction rate is very small. Also note that the distribution is unaffected in the D_2O case but is considerably steeper for the hardened spectrum in the AIR coolant case. This might be explained by the fact that a significant amount of (N,2N) reactions are going on in the D_2O coolant.

(16) The effect of using a different fission spectrum with transport corrected cross-sections since it applied to calculations made with the code WIMS was of particular interest. A number of ANISN cases were therefore run under these conditions. Table (XII) shows their effect on the (N,2N) reaction ratio.

Case #	F.S.	Source F.S.	Cool	N2NR(%)	$N2NR_1/N2NR$	$N2NR_2/N2NR$	$N2NR_3/N2NR$
22	238(1MeV)	235(.025eV)	D_2O	.09698	1.432	1.218	.840
28	238(1MeV)	235(1.43MeV)	D_2O	.13913	1.429	1.217	.841
26	234(1.43 MeV)	235(1.43MeV)	D_2O	.14228	1.433	1.219	.840
29	238(1MeV)	235(1.43MeV)	Air	.15762	1.365	1.197	.850
27	235(1.43 MeV)	234(1.43MeV)	Air	.16174	1.368	1.198	.849
30	238(1MeV)	235(.025eV)	D_2O	.10302	1.383	1.194	.858

TABLE XII: Transport Corrected Cross-Sections

It can be seen here that the effect of varying the fission spectrum is more pronounced, especially for the distribution of the (N,2N) reaction ratio, than it was for the fast fission ratio. This susceptibility can be explained by the high energy theshold of the (N,2N) reaction in uranium. Therefore a hardened fission spectrum will lead to more (N,2N) reactions; and if a hardened fission spectrum is used both in creating the fixed source of U235 fission neutrons and for generating the second generation neutrons in the high energy region, the effect is even larger.

(17) Geometry effects were also investigated with the Monte Carlo MORSE code. The different geometries in question here are the smeared annuli models of the CANDU fuel bundle which had to be used in ANISN since it is a one dimensional transport code. Also MORSE allows comparison with a very basically different method of simulating the neutron flux. TABLE (XIII) shows the different MORSE calculations for the (N,2N) reaction ratio using different geometries.

Case #	Geom.	Cool	N2NR(%)	$N2NR_1/N2NR$	$N2NR_2/N2NR$	$N2NR_3/N2NR$
17	ANN(equal thick)	D_2O	.11157	1.244	1.077	.928
18	PIN	D_2O	.10787	1.442	1.192	.849
21	ANN(equal thick)	Air	.12494	1.094	1.123	.932
20	ANN(exact)	Air	.11698	1.332	1.185	.871
ANISN						
30	ANN(equal thick)	D_2O	.10302	1.383	1.194	.858

TABLE XIII: Geometry Effects

The actual pin geometry of the fuel element can be simulated in MORSE since it is a 3 dimensional code. Cases with the same smeared annuli as in ANISN were run on MORSE. It can be seen from Table (13) that a difference of 3% results between the PIN and the equal thickness model. However the difference in (N,2N) ratio between a P8, S16, 6 groups, D_2O coolant ANISN run and the MORSE annular geometry 6 group run is of the order of 8% for 10^5 input particles. Note that the difference between the two methods is substantial even though they were using exactly the same cross section library. Transport theory also gave a much steeper distribution.

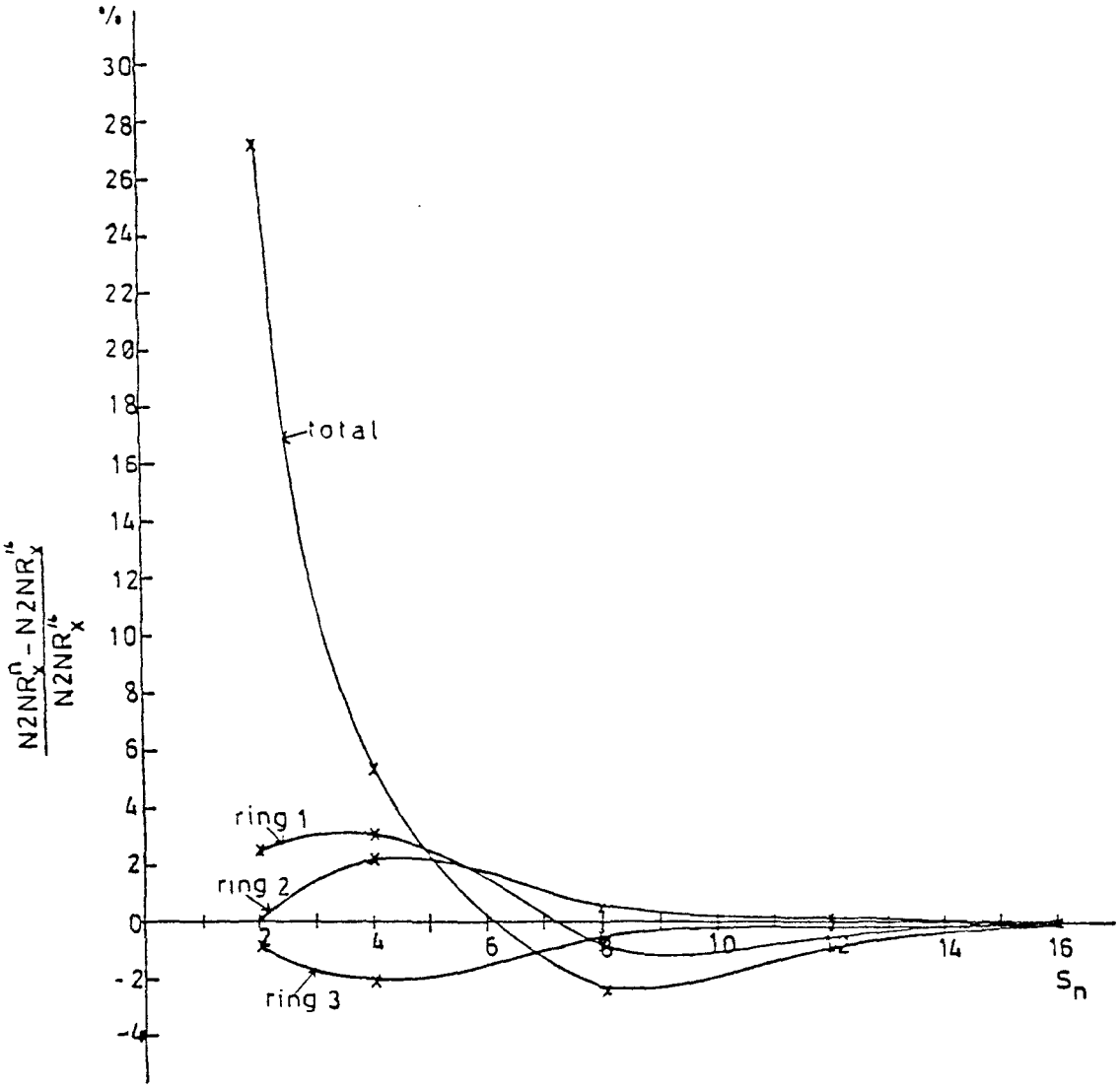

FIG. 19 Percent difference in the (N,2N) reaction ratio as a function of angular quadrature.

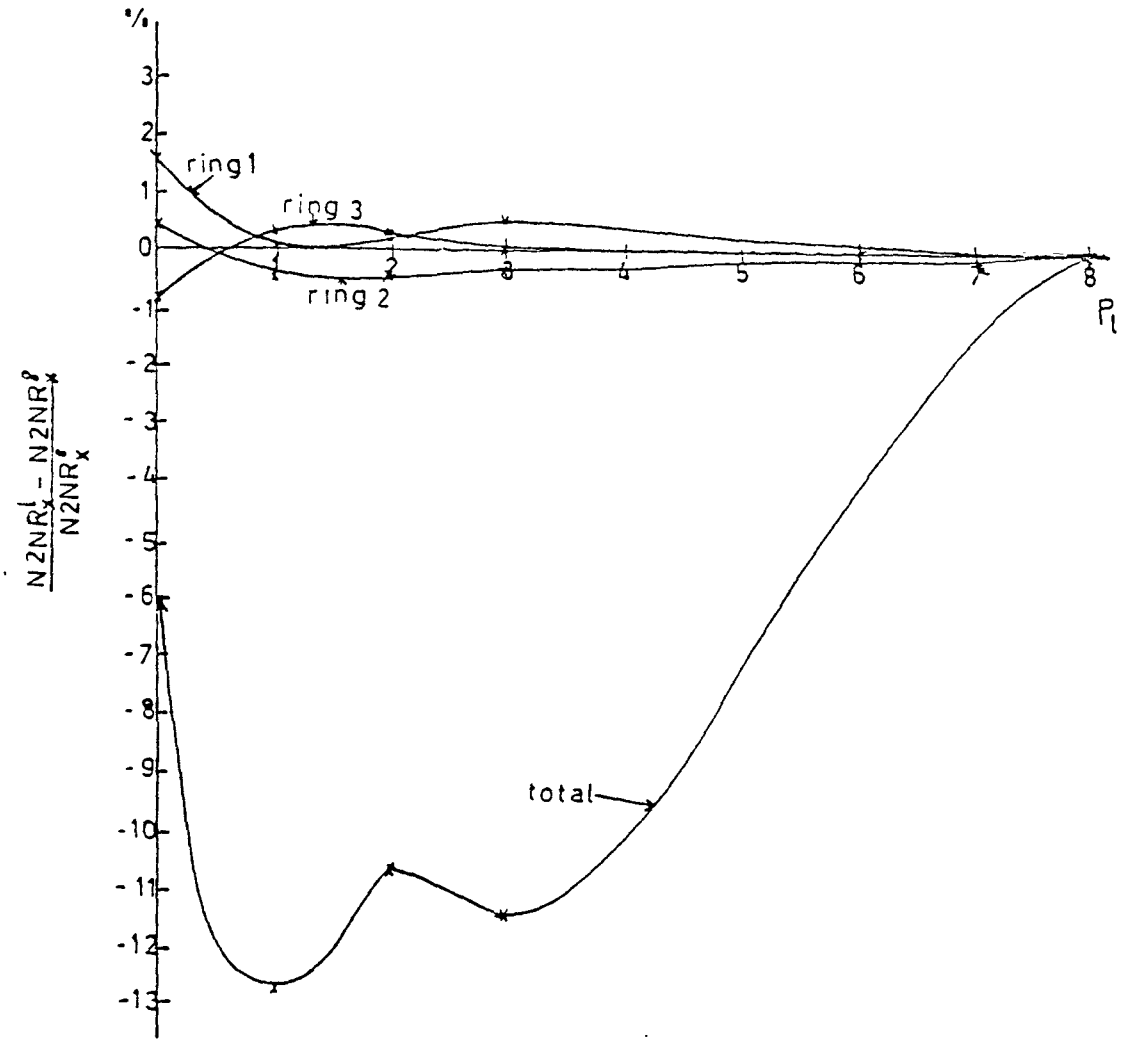

FIG. 11: Percent difference in the (N,2N) reaction ratio as a function of the order of the Legendre approximation.

The exact case refers to 2 different smeared annuli model in which the same area of fuel that exist on one side of a circle going through the center of the pins is conserved in the smeared annuli model. See Figure (2) for graphical representation. A difference of 6% was observed in the (N,2N) reaction ratio between the exact model and the model in which equal thicknesses of fuel is placed on each side of the center circles. This difference is larger than what was found in the case of the fast fission ratio. It would therefore require a few more cases investigating the particular aspect of the smearing.

(18) Cases with the heavy water coolant removed were also simulated. These so called AIR coolant runs allow us to look at what would happen to the fast fission ratio in a loss of coolant accident (LOCA). The (N,2N) reaction ratio is then of the order of 10% higher, thus contributing to a positive reactivity addition. The distribution (cases 5,6) of the (N,2N) reaction is also flatter for AIR coolant than D_2O coolant. This is due to the moderating effect of the heavy water coolant.

(19) A different lattice pitch has also been investigated. All the cases previously referred to had a pitch of 28 cm thus a moderator thickness of 8.351 cm associated with the cell. The other pitch considered was of 24 cm for a moderator thickness of 6.251 cm. This lattice tightening leads to an increase in the (N,2N) reaction ratio. The cases in Table XIV were run with a P_3 Legendre approximation and an S_4 angular quadrature.

Case #	Cool	Pitch	N2NR(%)	$N2NR_1/N2NR$	$N2NR_2/N2NR$	$N2NR_3/N2NR$
1	D_2O	28 cm	.09608	1.433	1.217	.841
4	Air	28 cm	.10919	1.469	1.232	.828
20	D_2O	24 cm	.10068	1.417	1.203	.847
21	Air	24 cm	.11540	1.355	1.201	.851

TABLE XIV: Lattice Tightening

It can be seen from Table XIV that the increase for the 24 cm pitch is about 4.8% for the D_2O coolant and of 5.7% for the AIR coolant case. The distribution of the (N,2N) ratio is also flatter for the tighter pitch.

(20) (N,2N) reactions also happen in the heavy water coolant and moderator. They contribute about .3% of the total flux of the CANDU reactor as compared to the (N,2N) reactions in the fuel which contribute only about .1% of the total flux. Out of the (N,2N) reactions occurring in heavy water about 80% of them will occur in the moderator. The rest of them are distributed as follows:
1% in the central coolant, 5% between the first and the second fuel annulus, 8.5% in the area between the second and the third fuel annuli and the remaining 5.5% between the third fuel annulus and the pressure tube.

The overall (N,2N) reaction rate in D_2O remains the same for the calculations with the two different energy meshes. Again the reaction ratio over the whole bundle goes down when white reflection with albedo = 0 is used.

CONCLUSION

It is possible to reproduce the Zed-II measurements of the Fast Fission Ratio to an accuracy of about 5% at best. However, the cross-sections data from the ENDF/B-IV tapes is not much more accurate than 2 to 3% especially for uranium (238) inelastic scattering.

It was found that an energy structure with 6 groups above 500 KeV was sufficient to estimate the Fast Fission Ratio. The order of the Legendre approximation had no effect on the distribution of fast fission across the fuel bundle but increased the overall value of the Fast Fission Ratio slightly. Increasing the order of the angular quadrature did not affect the overall value of the fast fission but flattened its distribution across the fuel bundle considerably. It is therefore advisable to spend ones computing money on higher Sn rather than higher Pn order.

It was also discovered that an energy mesh using 6 groups above 500 KeV (WIMS) was sufficiently small for the purposes of studying the fast fission. A spatial mesh of 56 intervals over the fuel bundle radial geometry was found to be sufficiently small for good flux convergence.

The reflective right hand boundary condition was found to give a higher value of fast fission ratio than the white reflection with albedo equal to one which in turn is much bigger than the value for albedo equal zero representing a single cell reactor. This is to be expected since the W/Alb = 0 does not include neither of the neutrons going outward of the fuel bundle which would have been reflected nor neutrons added to the fuel bundle under study coming from other cells.

Generating all the new generation neutrons according to the U235 (.025eV) fission spectrum was found to be adequate since the U238 fission spectrums do not vary very much with respect to the input neutron. However, by hardening the fission spectrum, that is to increase the average value of the temperature of the spectrum distribution, a considerably higher value of the Fast Fission Ratio is obtained. This higher value is much closer to the absolute value of the ratio measured experimentally but its distribution across the fuel bundle still is steeper.

The geometrical model used to simulate the fuel bundle was found to have a considerable influence on the Fast Fission Ratio. The Monte Carlo method showed that going from an equal thickness smeared annuli model to the exact pin distribution gave an approximately 3% decrease in the absolute value of the Fast Fission Ratio while the distribution got slightly steeper as you travel from the center of the fuel cell to the moderator.

Removing the heavy water coolant as in a LOCA increased the Fast Fission Ratio by as much as 20%. These results agreed very closely with what was obtained experimentally for similar conditions. When the coolant is replaced by air the distribution of the FFR becomes flatter.

Tightening the lattice pitch from 280 mm to 240 mm led to an increase of the Fast Fission Ratio of the order of 5% without much effect on the distribution. The values obtained for the tighter pitch agreed much better with the experimental results than for the wider pitch.

These calculations show that many factors can influence the value obtained for the Fast Fission Ratio if one is interested in a very precise value (order of 1%). But the most serious limitation remains the knowledge of precise cross-sections. It would be interesting to repeat these calculations as better cross-sections values become available.

APPENDIX

Included are tables showing the results for all the cases ran on both ANISN and MORSE. They cover the (N,2N) reactions in both the fuel and the heavy water regions. Only specific cases were pulled out of these tables as examples in the above discussion. The (N,2N) reaction ratio appears as a percent at the top. They also include a complete tabulation of all the fast fission ratio investigations.

It should be noted that the length of the fuel channel was assumed to be 50 cm in the ANISN calculations. In the MORSE calculations a reflective boundary condition was used at the ends, thus representing an effectively infinitely long fuel channel. In the Zed-II experiments a fuel channel length of 250 cm was used. These length discrepancies will lead to different buckling values which can explain some of the differences in the values calculated for the fast fission ratios between ANISN, MORSE and the experiments performed in Zed-II.

TABLE XV: TAPE SOURCE CATALOGUED

	PFN	Prog.	#Gr.	#Int.	Distr.	Spectrum	Pitch	Geom.	Cool.	Date
1	SOURCE	ANISN	100	56	Latrep	U235	28	ANN	D_2O	14/7
2	ESOU34	ANISN	34	56	Latrep	U235	28	ANN	D_2O	14/7
3	ESOU46	ANISN	46	56	Latrep	U235	28	ANN	D_2O	21/7
4	RDSO34	ANISN	34	56	AECL-2636	U235 (.025eV)	28	ANN	D_2O	25/7
5	RASO34	ANISN	34	56	AECL-2636	U235 (.025eV)	28	ANN	AIR	25/7
6	RDSO06	ANISN	6	56	AECL-2636	U235 (.025eV)	28	ANN	D_2O	25/7
7	RASO06	ANISN	6	56	AECL-2636	U235 (.025eV)	28	ANN	AIR	25/7
8	RDSOL6	ANISN	6	Latrep 26	AECL-2636	U235 (.025eV)	28	ANN	D_2O	5/8
9	RDS24	ANISN	6	56	AECL-2636	U235 (.025eV)	24	ANN	D_2O	22/8
10	AAS24	ANISN	6	56	AECL-2636	U235 (.025eV)	24	ANN	AIR	22/8
11	MORSOUR	MORSE	5	3	AECL-2636	U235 (.025eV)	28	ANN	D_2O	16/8
12	MPSOUR	MORSE	5	4	AECL-2636	U235 (.025eV)	28	PIN	D_2O	15/8
13	MASA28	MORSE	5	3	AECL-2636	U235 (.025eV)	28	ANN	AIR	23/8
14	MASP28	MORSE	5	4	AECL-2636	U235 (.025eV)	28	PIN	AIR	23/8
15	MDSA24	MORSE	5	3	AECL-2636	U235 (.025eV)	24	ANN	D_2O	22/8
16	MASA24	MORSE	5	3	AECL-2636	U235 (.025eV)	24	ANN	AIR	22/8
17	MDSP24	MORSE	5	4	AECL-2636	U235 (.025eV)	24	PIN	D_2O	23/8
18	MASP24	MORSE	5	4	AECL-2636	U235 (.025eV)	24	PIN	AIR	23/8
19	HADS28	ANISN	6	56	AECL-2636	U235 (1.43MeV)	28	ANN	D_2O	
20	HAAS28	ANISN	6	56	AECL-2636	U235 (1.43MeV)	28	ANN	AIR	

TABLE XVI: ANISN Calculations

	Gr.	Cool.	Alb.	Pn	Sn	Time	F.Y.R.	F.F.R.	$FYR._1$	FFR_1	FYR_2	FFR_2	FYR_3	FFR_3
1	6	D_2O	Ref	3	4	37.879	.057	.050	.083 (1.445)	.072 (1.445)	.070 (1.220)	.061 (1.220)	.048 (.837)	.042 (.837)
2	6	D_2O	Ref	8	4	39.79	.060	.052	.086 (1.443)	.075 (1.444)	.073 (1.221)	.063 (1.221)	.050 (.837)	.043 (.837)
3	6	D_2O	Ref	3	4*	37.52	.058	.051	.084 (1.435)	.073 (1.436)	.071 (1.216)	.062 (1.216)	.049 (.841)	.043 (.840)
4	6	Air	Ref	3	4	39.71	.067	.058	.093 (1.381)	.081 (1.382)	.081 (1.202)	.070 (1.202)	.057 (.844)	.049 (.844)
5	34	Air	Ref	3	4	232.09	.067	.058	.092 (1.368)	.080 (1.380)	.080 (1.191)	.069 (1.194)	.056 (.838)	.049 (.845)
6	34	D_2O	Ref	3	4	209.07	.057	.050	.083 (1.442)	.072 (1.443)	.070 (1.219)	.061 (1.220)	.048 (.838)	.042 (.838)
7	34	D_2O	Ref	8	4	222.9	.060	.052	.086 (1.441)	.074 (1.442)	.073 (1.221)	.063 (1.221)	.050 (.838)	.043 (.838)
8	6	D_2O	Ref	3	12	262.4	.060	.052	.084 (1.401)	.073 (1.401)	.072 (1.199)	.062 (1.120)	.051 (.853)	.044 (.853)
9	6	D_2O	Ref	8	12	269.41	.060	.052	.084 (1.400)	.073 (1.401)	.072 (1.199)	.062 (1.199)	.051 (.853)	.044 (.853)
10	6	D_2O	Ref	8	8	150.97	.059	.051	.083 (1.409)	.072 (1.410)	.071 (1.203)	.062 (1.203)	.050 (.850)	.044 (.850)
11	34	D_2O	Ref	3	12	990.69	.060	.052	.083 (1.398)	.072 (1.399)	.071 (1.198)	.062 (1.199)	.051 (.854)	.044 (.854)
12	6	D_2O	Ref	0	4	41.32	.062	.054	.091 (1.459)	.079 (1.459)	.077 (1.228)	.063 (1.228)	.052 (.832)	.045 (.832)
13	6	D_2O	Ref	1	4	36.72	.056	.049	.081 (1.440)	.071 (1.441)	.069 (1.218)	.060 (1.219)	.047 (.839)	.041 (.839)
14	6	D_2O	White 1.0	3	4	33.08	.057	.050	.082 (1.446)	.072 (1.447)	.070 (1.221)	.061 (1.221)	.048 (.837)	.042 (.837)
15	6	D_2O	Ref	3	2	23.59	.129	.112	.168 (1.305)	.147 (1.304)	.151 (1.177)	.133 (1.178)	.113 (.878)	.099 (.878)

TABLE XVI : ANISN Calculations (Continued)

	Gr.	Cool.	Alb.	Pn	Sn	Time	F.Y.R.	F.F.R.	$FYR._1$	FFR_1	FYR_2	FFR_2	FYR_3	FFR_3
16	6	D_2O	Ref	2	4	-----	.058	.050	.083 (1.440)	.072 (1.441)	.070 (1.219)	.061 (1.219)	.048 (.838)	.042 (.838)
17	6	D_2O	White 0.0	3	4	10.22	.055	.048	.081 (1.453)	.070 (1.454)	.068 (1.224)	.059 (1.224)	.046 (.833)	.040 (.834)
18	6	D_2O	Ref	Diff	4	3.88	.040	.035	.061 (1.518)	.053 (1.518)	.050 (1.253)	.044 (1.253)	.033 (.812)	.028 (.812)
19	6	D_2O (Latrep	Ref Mesh)	3	4	15.83	.056	.049	.081 (1.453)	.071 (1.453)	.069 (1.231)	.060 (1.231)	.047 (.832)	.040 (.831)
20	6	D_2O P=24	Ref	3	4	33.04	.060	.052	.085 (1.431)	.074 (1.431)	.072 (1.205)	.063 (1.207)	.050 (.843)	.044 (.843)
21	6	Air P=24	Ref	3	4	39.63	.070	.061	.096 (1.368)	.084 (1.369)	.085 (1.207)	.074 (1.207)	.059 (.846)	.052 (.846)
22	6	D_2O P=28	Ref	0 T.C.	4	16.486	.059	.051	.085 (1.444)	.074 (1.444)	.072 (1.221)	.063 (1.221)	.049 (.837)	.043 (.837)
23	6	D_2O P=24	Ref	0 T.C.	4	13.045	.061	.053	.087 (1.431)	.076 (1.431)	.074 (1.208)	.064 (1.209)	.051 (.842)	.045 (.842)
24	6	D_2O P=28	Ref (235 F.S.)	3	4	37.926	.058	.050	.083 (1.445)	.072 (1.445)	.070 (1.220)	.061 (1.220)	.048 (.837)	.042 (.837)
25	6	Air P=28	Ref (235 F.S.)	3	4	39.747	.067	.058	.093 (1.381)	.081 (1.381)	.081 (1.202)	.070 (1.202)	.057 (.845)	.049 (.844)
26	6	D_2O P=28	Ref (235 F.S.)	0 T.C.	4 Hard Source Spectrum	14.835	.065	.056	.094 (1.444)	.081 (1.445)	.080 (1.221)	.069 (1.221)	.054 (.837)	.047 (.837)
27	6	Air P=28	Ref (235 F.S.)	0 T.C.	4 Hard Source Spectrum	14.876	.076	.065	.104 (1.375)	.090 (1.376)	.091 (1.200)	.078 (1.200)	.064 (.846)	.055 (.846)
28	6	D_2O P=28	Ref	0 T.C.	4 Hard Source Spectrum	14.791	.065	.056	.093 (1.443)	.081 (1.444)	.079 (1.221)	.068 (1.221)	.054 (.837)	.047 (.837)

TABLE XVI: ANISN Calculations (Continued)

	Gr.	Cool.	Alb.	Pn	Sn	Time	F.Y.R.	F.F.R.	$FYR._1$	FFR_1	FYR_2	FFR_2	FYR_3	FFR_3
29	6	Air P=28	Ref	0 T.C.	4 Hard Source Spectrum	14.750	.075	.065	.103 (1.375)	.089 (1.375)	.090 (1.200)	.078 (1.200)	.064 (.847)	.055 (.846)
30	6	D_2O	Ref	8	16	-----	.060	.052	.084 (1.398)	.073 (1.398)	.072 (1.198)	.062 (1.198)	.051 (.854)	.045 (.854)

TABLE XVII: MORSE Calculations

	Geom.	Cool.	Sn	Alb.	#Part.	FYR	FFR	FYR_1	FFR_1	FYR_2	FFR_2	FYR_3	FFR_3
1	ANN	D_2O	4	0.0	10^4	.061	.054	.083 (1.348)	.072 (1.344)	.082 (1.330)	.072 (1.347)	.059 (.811)	.043 (.805)
2	PIN	D_2O	4	0.0	10^4	.061	.053	.103 (1.680)	.091 (1.707)	.073 (1.188)	.063 (1.185)	.050 (.809)	.043 (.806)
3	ANN	D_2O	4	1.0	10^4	.063	.054	.081 (1.301)	.071 (1.307)	.076 (1.211)	.066 (1.209)	.054 (.866)	.047 (.866)
4	PIN	D_2O	4	1.0	10^4	.060	.053	.084 (1.388)	.073 (1.395)	.077 (1.271)	.067 (1.270)	.050 (.827)	.043 (.827)
5	ANN	Air	4	1.0	10^4	.072	.062	.091 (1.272)	.079 (1.272)	.086 (1.201)	.075 (1.201)	.062 (.865)	.053 (.866)
6	PIN	Air	8	1.0	10^4	.070	.061	.095 (1.363)	.083 (1.354)	.085 (1.221)	.074 (1.222)	.059 (.840)	.051 (.841)
7	ANN	D_2O	4	0.0	10^4	.060	.052	.084 (1.405)	.073 (1.404)	.069 (1.160)	.060 (1.162)	.052 (.868)	.045 (.867)
8	ANN	D_2O	8	1.0	10^4	.063	.055	.090 (1.417)	.078 (1.414)	.072 (1.132)	.062 (1.135)	.055 (.876)	.048 (.876)
9	ANN	D_2O	12	1.0	10^4	.063	.055	.090 (1.417)	.078 (1.414)	.072 (1.132)	.062 (1.135)	.055 (.876)	.048 (.876)
10	PIN	Air	8	1.0	10^4	.072	.063	.101 (1.398)	.088 (1.403)	.091 (1.259)	.079 (1.259)	.060 (.830)	.052 (.829)
11	PIN	D_2O	8	1.0	10^4	.062	.054	.089 (1.423)	.077 (1.422)	.076 (1.221)	.066 (1.225)	.052 (.841)	.045 (.839)
12	PIN	D_2O	12	1.0	10^4	.062	.054	.089 (1.423)	.077 (1.422)	.076 (1.221)	.066 (1.225)	.052 (.841)	.045 (.839)
13	ANN	D_2O P=24	8	1.0	10^4	.067	.058	.091 (1.370)	.079 (1.374)	.077 (1.150)	.067 (1.150)	.058 (.876)	.051 (.875)
14	ANN	Air P=24	8	1.0	10^4	.076	.066	.104 (1.368)	.091 (1.374)	.085 (1.121)	.074 (1.124)	.067 (.881)	.058 (.878)
15	PIN	D_2O P=24	8	1.0	10^4	.065	.056	.092 (1.417)	.080 (1.428)	.077 (1.192)	.067 (1.196)	.055 (.851)	.048 (.848)

TABLE XVII: MORSE Calculations (Continued)

	Geom.	Cool.	Sn	Alb.	#Part.	FYR	FFR	FYR_1	FFR_1	FYR_2	FFR_2	FYR_3	FFR_3
16	PIN	Air P=24	8	1.0	10^4	.074	.064	.097 (1.311)	.085 (1.312)	.087 (1.170)	.075 (1.167)	.065 (.872)	.056 (.873)
17	ANN	D_2O P=28	5	1.0	99999	.063	.055	.084 (1.331)	.073 (1.334)	.074 (1.164)	.064 (1.166)	.056 (.879)	.048 (.878)
18	PIN	D_2O P=28	5	1.0	99999	.062	.053	.086 (1.393)	.074 (1.393)	.075 (1.211)	.065 (1.212)	.052 (.850)	.045 (.850)
19	ANN	Air P=28	5	1.0	10^4	.072	.063	.096 (1.327)	.084 (1.336)	.086 (1.183)	.074 (1.180)	.062 (.863)	.054 (.862)
20	ANN Exact	Air P=28	5	1.0	99999	.071	.062	.098 (1.375)	.085 (1.375)	.083 (1.173)	.073 (1.174)	.062 (.868)	.054 (.867)
21	ANN	Air P=28	5	1.0	99999	.072	.062	.091 (1.273)	.079 (1.277)	.082 (1.148)	.071 (1.149)	.064 (.887)	.055 (.886)
22	PIN MASP	Air P=28	5	1.0	99999	.070	.061	.094 (1.339)	.082 (1.337)	.085 (1.203)	.074 (1.204)	.060 (.852)	.052 (.852)
23	ANN MDSA	D_2O P=24	5	1.0	99999	.066	.058	.090 (1.351)	.079 (1.363)	.076 (1.143)	.066 (1.144)	.058 (.880)	.051 (.880)
24	ANN MASA	Air P=24	5	1.0	99999	.077	.067	.101 (1.309)	.088 (1.308)	.089 (1.152)	.078 (1.154)	.068 (.879)	.059 (.879)
25	PIN MDSP	D_2O P=24	5	1.0	99999	.066	.057	.092 (1.391)	.080 (1.391)	.079 (1.200)	.069 (1.200)	.056 (.853)	.049 (.853)
26	PIN MASP	Air P=24	5	1.0	99999	.076	.066	.100 (1.323)	.087 (1.324)	.090 (1.185)	.078 (1.185)	.065 (.863)	.057 (.863)

TABLE XVIII: WIMS Calculations

	Geom.	Cool.	Type	Time	FYR	FFR	FYR_1	FFR_1	FYR_2	FFR_2	FYR_3	FFR_3
1	DSN	D_2O	INF.	13.062	.058	.049	.085 (1.477)	.073 (1.478)	.069 (1.205)	.060 (1.205)	.048 (.839)	.041 (.838)
			EFF.		.064	.055	.094 (1.475)	.081 (1.476)	.077 (1.204)	.066 (1.205)	.054 (.839)	.046 (.839)
2	DSN	Air	INF.	12.089	.065	.056	.092 (1.412)	.079 (1.414)	.078 (1.196)	.067 (1.197)	.055 (.845)	.047 (.845)
			EFF.		.072	.062	.102 (1.411)	.088 (1.412)	.086 (1.196)	.074 (1.196)	.061 (.845)	.053 (.845)
3	PIJ	D_2O	INF.	73.538	.057	.049	.080 (1.405)	.070 (1.426)	.068 (1.193)	.058 (1.190)	.049 (.853)	.042 (.850)
			EFF.		.063	.054	.088 (1.404)	.076 (1.405)	.075 (1.192)	.064 (1.193)	.054 (.853)	.046 (.853)
4	PIJ	Air	INF.	74.248	.064	.055	.086 (1.343)	.074 (1.343)	.076 (1.187)	.065 (1.188)	.055 (.858)	.047 (.858)
			EFF.		.071	.061	.095 (1.341)	.082 (1.342)	.084 (1.187)	.072 (1.187)	.061 (.859)	.052 (.858)

TABLE XIX: ANISN Calculations

(N,2N) in Uranium 238/Reactor Power

#	Gr.	Cool.	Alb.	Pn	Sn	Time	$\%(N,2N)_T$	$\%(N,2N)_1$	$\%(N,2N)_2$	$\%(N,2N)_3$
1	6	D_2O	Ref.	3	4	37.879	.096	.138 (1.433)	.117 (1.217)	.081 (.841)
2	6	D_2O	Ref.	8	4	39.79	.109	.155 (1.426)	.133 (1.221)	.091 (.841)
3	6	D_2O	Ref.	3	4*	37.52	.098	.139 (1.424)	.119 (1.213)	.082 (.844)
4	6	Air	Ref.	3	4	39.71	.109	.160 (1.469)	.135 (1.232)	.090 (.828)
5	34	Air	Ref.	3	4	232.09	.126	.173 (1.368)	.151 (1.197)	.107 (.849)
6	34	D_2O	Ref.	3	4	209.07	.112	.159 (1.430)	.136 (1.216)	.094 (.841)
7	34	D_2O	Ref.	8	4	222.9	.129	.183 (1.422)	.157 (1.221)	.108 (.841)
8	6	D_2O	Ref.	3	12	262.4	.102	.141 (1.384)	.121 (1.195)	.087 (.858)
9	6	D_2O	Ref.	8	12	269.41	.102	.141 (1.385)	.122 (1.195)	.087 (.857)
10	6	D_2O	Ref.	8	8	150.97	.100	.140 (1.394)	.120 (1.199)	.086 (.854)
11	34	D_2O	Ref.	3	12	990.67	.118	.163 (1.382)	.141 (1.194)	.101 (.858)
12	6	D_2O	Ref.	0	4	41.32	.102	.148 (1.448)	.125 (1.226)	.085 (.834)
13	6	D_2O	Ref.	1	4	36.72	.095	.135 (1.426)	.115 (1.215)	.080 (.843)
14	6	D_2O	White 1.0	3	4	33.08	.095	.136 (1.435)	.116 (1.218)	.080 (.840)
15	6	D_2O	Ref.	3	2	23.59	.131	.186 (1.419)	.157 (1.195)	.112 (.851)
16	6	D_2O	Ref.	2	4	-----	.097	.138 (1.428)	.118 (1.216)	.082 (.842)
17	6	D_2O	White 0.0	3	4	10.22	.091	.132 (1.445)	.112 (1.223)	.076 (.836)
18	6	D_2O	Ref.	Dif.	4	3.88	.063	.095 (1.499)	.078 (1.244)	.052 (.819)

TABLE XIX: ANISN Calculations

(Continued)

#	Gr.	Cool.	Alb.	Pn	Sn	Time	% $(N,2N)_T$	% $(N,2N)_1$	% $(N,2N)_2$	% $(N,2N)_3$
19	6	D_2O (Latrep mesh)	Ref.	3	4	15.83	.094	.135 (1.440)	.115 (1.228)	.078 (.835)
20	6	D_2O D=24	Ref.	3	4	33.04	.101	.143 (1.417)	.121 (1.203)	.085 (.847)
21	6	Air P=24	Ref.	3	4	39.63	.115	.156 (1.355)	.139 (1.201)	.098 (.851)
22	6	D_2O P=28	Ref.	0	4	16.486	.097	.139 (1.432)	.118 (1.218)	.082 (.840)
23	6	D_2O P=24	Ref.	0	4	13.045	.101	.143 (1.417)	.122 (1.204)	.086 (.847)
24	6	D_2O P=28	Ref. (235	3 FS)	4	37.926	.096	.138 (1.433)	.117 (1.217)	.081 (.840)
25	6	Air P=28	Ref. (235	3 FS)	4	39.747	.109	.150 (1.369)	.131 (1.197)	.093 (.849)
26	6	D_2O P=28	Ref. (235 FS)	0 TC	4	14.835	.142	.204 (1.433)	.173 (1.219)	.120 (.840)
27	6	Air P=28	Ref. (235 FS)	0 TC	4	14.876	.162	.221 (1.368)	.194 (1.198)	.137 (.849)
28	6	D_2O P=28	Ref.	0 TC	4	14.791	.139	.199 (1.429)	.169 (1.217)	.117 (.841)
29	6	Air P=28	Ref.	0 TC	4	14.750	.158	.215 (1.365)	.189 (1.197)	.134 (.850)
30	6	D_2O	Ref.	8	16		.103	.142 (1.383)	.123 (1.194)	.088 (.858)

TABLE XX: MORSE Calculations

#	Geom.	Cool.	Sn	Alb.	#Part.	$(N,2N)_T$	$(N,2N)_1$	$(N,2N)_2$	$(N,2N)_3$	FIX SOURCE
1	ANN	D_2O	4	0.0	10^4	.095	.112 (1.174)	.110 (1.156)	.086 (.909)	
2	PIN	D_2O	4	0.0	10^4	.099	.138 (1.397)	.117 (1.190)	.085 (.857)	
3	ANN	D_2O	4	1.0	10^4	.108	.125 (1.155)	.148 (1.369)	.090 (.830)	
4	PIN	D_2O	4	1.0	10^4	.091	.122 (1.339)	.113 (1.235)	.078 (.850)	
5	ANN	AIR	4	1.0	10^4	.122	.171 (1.403)	.158 (1.293)	.098 (.803)	
6	PIN	AIR	8	1.0	10^4	.114	.208 (1.823)	.126 (1.101)	.092 (.802)	
7	ANN	D_2O	4	0.0	10^4	.103	.154 (1.497)	.122 (1.181)	.087 (.843)	
8	ANN	D_2O	8	1.0	10^4	.105	.184 (1.748)	.098 (.930)	.095 (.898)	
9	ANN	D_2O	12	1.0	10^4	.105	.184 (1.748)	.098 (.930)	.095 (.898)	
10	PIN	AIR	8	1.0	10^4	.120	.142 (1.182)	.144 (1.200)	.107 (.891)	
11	PIN	D_2O	8	1.0	10^4	.107	.163 (1.521)	.113 (1.060)	.095 (.866)	
12	PIN	D_2O	12	1.0	10^4	.107	.163 (1.521)	.113 (1.060)	.095 (.866)	
13	ANN	D_2O P=24	8	1.0	10^4	.129	.172 (1.339)	.148 (1.150)	.113 (.881)	
14	ANN	AIR P=24	8	1.0	10^4	.127	.141 (1.110)	.131 (1.030)	.123 (.967)	
15	PIN	D_2O P=24	8	1.0	10^4	.114	.110 (.965)	.110 (.967)	.116 (1.019)	
16	PIN	AIR P=24	8	1.0	10^4	.125	.162 (1.295)	.167 (1.331)	.101 (.809)	
17	ANN	D_2O P=28	5	1.0	99,999	.112	.139 (1.244)	.120 (1.077)	.103 (.928)	
18	PIN	D_2O P=28	5	1.0	99,999	.108	.156 (1.442)	.129 (1.192)	.092 (.849)	

TABLE XXI: MORSE Calculations

(Continued)

#	Geom.	Cool.	Sn	Alb.	#Part.	$(N,2N)_T$	$(N,2N)_1$	$(N,2N)_2$	$(N,2N)_3$	FIX SOURCE
19	ANN	AIR P=28	5	1.0	10^4	.136	.150 (1.097)	.177 (1.302)	.117 (.858)	
20	ANN Exact	AIR P=28	5	1.0	99,999	.117	.156 (1.332)	.139 (1.185)	.102 (.871)	
21	ANN	AIR	5	1.0	99,999	.125	.137 (1.094)	.140 (1.123)	.116 (.932)	MASA
22	PIN	AIR	5	1.0	99,999	.120	.176 (1.470)	.137 (1.147)	.102 (.850)	MASP
23	ANN	D_2O	5	1.0	99,999	.117	.154 (1.315)	.129 (1.099)	.106 (.906)	MDSA
24	ANN	AIR	5	1.0	99,999	.136	.187 (1.375)	.149 (1.094)	.121 (.891)	MASA
25	PIN	D_2O	5	1.0	99,999	.116	.170 (1.467)	.131 (1.133)	.100 (.866)	MDSP
26	PIN	AIR	5	1.0	99,999	.134	.172 (1.288)	.158 (1.182)	.116 (.871)	MASP

REFERENCES

(1) DeLange, P.Q.; Bigham, C.B.; Green, R.E.; Manuel, T.J. "Experimental Initial Conversion and Fast Fission Ratios for Clusters of Natural U and UO_2 in D_2O", AECL-2636, Atomic Energy of Canada Ltd., Chalk River, Canada (1966).

(2) Wright, R.Q.; Greene, N.M.; Lucius, J.L.; Craven, C.W. Jr. "SUPERTOG: A Program to Generate Fine Group Constants and Pn Scattering Matrices from ENDF/B", ORNL-TM-2679, Oak Ridge National Laboratory, Oak Ridge, Tennessee (1969).

(3) Engle, W.W. Jr. "A Users Manual for ANISN: A One Dimensional Discrete Ordinates Transport Code with Anisotropic Scattering", K1693, Oak Ridge National Laboratory, Oak Ridge, Tennessee (1967).

(4) Drake, N.K. "Data Formats and Procedures for the ENDF Neutron Cross-Section Library", Brookhaven National Laboratory, Upton, New York (1973).

(5) Straker, E.A.; Stevens, P.N.; Irving, D.C.; Cain, V.R. "The MORSE Code - A Multi-group Neutron and Gamma Ray Transport Code", ORNL, Oak Ridge National Laboratory, Oak Ridge, Tennessee (1970).

(6) Greenspan, H.; Kelber, C.N.; Okrent, D. "Computing Methods in Reactor Physics", Gordon and Breach, New York, USA (1968).

(7) Roth, M.J.; MacDougall, J.D.; Kemshell, P.B. "The Preparation of Input Data for WIMS", AEEW-R538.

(8) Stone, T.W. "Time Dependant Studies of a 19-Element CANDU Fuel Bundle in the Blanket of a Thermonuclear Reactor", McMaster University (1977).

(9) Clark, H.K.; Hootman, H.E.; "ANISN-SRL", DPST-70-233, Savannah River Laboratory, Aikur, South Carolina (1970).